6 Quantum Tomography from Incomplete Data via *MaxEnt* Principle

Vladimír Bužek[1,2]

[1] Research Center for Quantum Information, Institute of Physics, Slovak Academy of Sciences, Dúbravská cesta 9, 845 11 Bratislava, Slovakia
[2] Faculty of Informatics, Masaryk University, Botanická 68a, 602 00 Brno, Czech Republic, buzek@savba.sk

> *...existing quantum theory must be supplemented with some principle that tells us how to translate, or encode, the results of measurements into a definite state description $\hat{\rho}$. Note that the problem is not to find $\hat{\rho}$ which correctly describes "true physical situation". That is unknown, and always remains so, because of incomplete information. In order to have a usable theory we must ask the much more modest question: What $\hat{\rho}$ best describes our state of knowledge about the physical situation?*
>
> E. T. Jaynes [1]

Abstract. We show how the maximum entropy (*MaxEnt*) principle can be efficiently used for a reconstruction of states of quantum systems from incomplete tomographic data. This *MaxEnt* reconstruction scheme can be in specific cases several orders of magnitude more efficient than the standard inverse Radon transformation or the reconstruction via direct sampling using pattern functions. We apply the MaxEnt algorithm for a reconstruction of motional quantum states of neutral atoms. As an example we analyze the experimental data obtained by the group of C. Salomon at the ENS in Paris and we reconstruct Wigner functions of motional quantum states of Cs atoms trapped in an optical lattice. We also reconstruct Wigner functions of a cavity field based on a measurement of the parity operator. We analyze in detail experimental data obtained by the group of S. Haroche at the ENS in Paris.

6.1 Modest Question

The concept of a quantum state represents one of the most fundamental pillars of the paradigm of quantum theory [2–4]. Contrary to its mathematical elegance and convenience in calculations, the physical interpretation of a quantum state is not so transparent. The problem is that the quantum state (described either by a state vector, or density operator or a phase-space probability density distribution) does not have a well-defined objective

V. Bužek, Quantum Tomography from Incomplete Data via *MaxEnt* Principle, Lect. Notes Phys. **649**, 189–234 (2004)
http://www.springerlink.com/

status, i.e. a state vector is not an *objective* property of a particle. According to Peres (see [2], pp. 373-374): "...there is no physical evidence whatsoever that every physical system has at every instant a well-defined state... In a strict interpretation of quantum theory these mathematical symbols [i.e., state vectors] represent *statistical information* enabling us to compute the *probabilities* of occurrence of specific events." Once this point of view is adopted then it becomes clear that any reconstruction of a density operator (or its mathematical equivalent) can be understood exclusively as an expression of our knowledge about the quantum mechanical state based on a certain set of measured data. To be more specific, any quantum-mechanical reconstruction scheme is nothing more than an *a posteriori* estimation of the density operator of a quantum-mechanical (microscopic) system based on data obtained with the help of a macroscopic measurement apparatus [4]. The quality of the reconstruction depends on the "quality" of the measured data and the efficiency of the reconstruction procedure with the help of which the data analysis is performed. In general, we can specify three different situations:

- Firstly, when all system observables are precisely measured. In this case the *complete reconstruction* of an initially unknown state can be performed. We can call this the reconstruction on the *complete* observation level. A typical example is a tomographic reconstruction of quantum states of light as discussed in Sect. 6.2 of this chapter.
- Secondly, when just part of the system observables is precisely measured then one cannot perform a complete reconstruction of the measured state. Nevertheless, the reconstructed density operator still uniquely determines mean values of the measured observables. We can denote this scheme as reconstruction on *incomplete* observation levels. In this chapter we will investigate in detail this specific situation and we will present a very efficient method of reconstruction of quantum states based on the principle of *Maximum entropy* (MaxEnt).
- Finally, when measurement does not provide us with sufficient information to specify the exact mean values (or probability distributions) but only frequencies of appearances of eigenstates of the measured observables, then one can perform an estimation (reconstruction) using methods such as maximum likelihood estimation (see [5]) or quantum Bayesian inference (see, for instance, the recent review [6]).

6.2 Complete Observation Level

Providing all system observables (i.e., the quorum [2, 4]) have been precisely measured, then the density operator of a quantum-mechanical system can be completely reconstructed (i.e., the density operator can be uniquely determined based on the available data). In principle, we can consider two different

schemes for reconstruction of the density operator of the given quantum-mechanical system. The difference between these two schemes is based on the way in which information about the quantum-mechanical system is obtained. The first type of measurement is such that on each element of the ensemble of the measured states only a *single* observable is measured. In the second type of measurement a *simultaneous* measurement of conjugate observables is assumed. We note that in both cases we will assume ideal, i.e., unit-efficiency, measurements. In what follows as an illustration we will consider a specific complete observation level that is realized via a quantum homodyne tomography of a single-mode electromagnetic field.

6.2.1 Quantum States of Light

Utilizing a close analogy between the operator for the electric component $\hat{E}(r,t)$ of a monochromatic light field and the quantum-mechanical harmonic oscillator we will consider a dynamical system that is described by a pair of canonically conjugated Hermitean observables $\hat{q}$ and $\hat{p}$,

$$[\hat{q},\hat{p}] = i\hbar. \tag{6.1}$$

Eigenvalues of these operators range continuously from $-\infty$ to $+\infty$. The annihilation and creation operators $\hat{a}$ and $\hat{a}^\dagger$ can be expressed as a complex linear combination of $\hat{q}$ and $\hat{p}$:

$$\hat{a} = \frac{1}{\sqrt{2\hbar}}\left(\lambda\hat{q} + i\lambda^{-1}\hat{p}\right); \qquad \hat{a}^\dagger = \frac{1}{\sqrt{2\hbar}}\left(\lambda\hat{q} - i\lambda^{-1}\hat{p}\right), \tag{6.2}$$

where λ is a real parameter. The operators $\hat{a}$ and $\hat{a}^\dagger$ obey the Weyl-Heisenberg commutation relation

$$[\hat{a},\hat{a}^\dagger] = 1, \tag{6.3}$$

and therefore possess the same algebraic properties as the operator associated with the complex amplitude of a harmonic oscillator (in this case $\lambda = \sqrt{m\omega}$, where m and ω are the mass and the frequency of the quantum-mechanical oscillator, respectively) or the photon annihilation and creation operators of a single mode of the quantum electromagnetic field. In this case $\lambda = \sqrt{\epsilon_0\omega}$ (ϵ_0 is the dielectric constant and ω is the frequency of the field mode) and the operator for the electric field reads (we do not take into account polarization of the field)

$$\hat{E}(r,t) = \sqrt{2}\mathcal{E}_0\left(\hat{a}\mathrm{e}^{-i\omega t} + \hat{a}^\dagger\mathrm{e}^{i\omega t}\right)u(r), \tag{6.4}$$

where $u(r)$ describes the spatial field distribution and is the same in both classical and quantum theories. The constant $\mathcal{E}_0 = (\hbar\omega/2\epsilon_0 V)^{1/2}$ is equal to the "electric field per photon" in the cavity of volume V.

6.2.2 Wigner Functions

In general, states of a quantum mechanical system are described by positive Hermitean density operators $\hat{\rho} = \hat{\rho}^{\dagger}$ that act on a Hilbert space H. The density operators $\hat{\rho}$ form a convex space $\mathcal{S}$. The extreme points of this state space correspond to a manifold of all one-dimensional projectors (pure states) acting on the given Hilbert space H. In the case of a harmonic oscillator one can introduce a quasi-probability density distributions in a phase space that can be associated with density operators (states) of the oscillator under consideration. In particular, the Wigner function [7, 8] can be defined as a particular Fourier transform of the density operator $\hat{\rho}$ of a harmonic oscillator expressed in the basis of the eigenvectors $|q\rangle$ of the position operator $\hat{q}$:

$$W_{\hat{\rho}}(q,p) \equiv \int_{-\infty}^{\infty} d\zeta \langle q - \zeta/2|\hat{\rho}|q + \zeta/2\rangle \mathrm{e}^{ip\zeta/\hbar}. \tag{6.5}$$

Alternatively, the Wigner function (WF) can be rewritten in the form

$$W_{\hat{\rho}}(q,p) = \frac{1}{2\pi\hbar} \int dp'\, dq'\, C_{\hat{\rho}}^{(W)}(q',p') \, \exp\left[-\frac{i}{\hbar}(qp' - pq')\right] , \tag{6.6}$$

where the characteristic function $C_{\hat{\rho}}^{(W)}(q,p)$ is given by the relation

$$C_{\hat{\rho}}^{(W)}(q,p) = \mathrm{Tr}\left[\hat{\rho}\hat{D}(q,p)\right]. \tag{6.7}$$

The displacement operator $\hat{D}(q,p)$ in terms of the position and the momentum operators reads

$$\hat{D}(q,p) = \exp\left[\frac{i}{\hbar}(\hat{q}p - \hat{p}q)\right]. \tag{6.8}$$

The Wigner function can be interpreted as the quasi-probability density distribution through which a probability can be expressed to find a quantum-mechanical system (harmonic oscillator) around the "point" (q,p) of the phase space. With the help of the Wigner function $W_{\hat{\rho}}(q,p)$ the position and momentum probability distributions $w_{\hat{\rho}}(q)$ and $w_{\hat{\rho}}(p)$ can be expressed from $W_{\hat{\rho}}(q,p)$ via marginal integration over the conjugated variable (in what follows we assume $\lambda = 1$)

$$w_{\hat{\rho}}(q) \equiv \frac{1}{\sqrt{2\pi\hbar}} \int dp\, W_{\hat{\rho}}(q,p) = \sqrt{2\pi\hbar}\langle q|\hat{\rho}|q\rangle, \tag{6.9}$$

where $|q\rangle$ is the eigenstate of the position operator $\hat{q}$. The marginal probability distribution $W_{\hat{\rho}}(q)$ is normalized to unity, i.e.,

$$\frac{1}{\sqrt{2\pi\hbar}} \int dq\, w_{\hat{\rho}}(q) = 1. \tag{6.10}$$

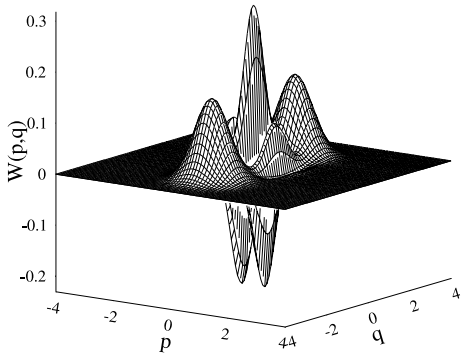

Fig. 6.1. The Wigner function of the even coherent state with $\alpha = 2$.

As an illustration, let us consider a Wigner function of a specific superposition of two coherent states:

$$|\alpha_{\rm e}\rangle = N_e^{1/2}\left(|\alpha\rangle + |-\alpha\rangle\right); \qquad N_e^{-1} = 2\left[1+\exp(-2|\alpha|^2)\right], \quad (6.11)$$

which is called the even coherent state [9]. The coherent state $|\alpha\rangle$ is defined as usually, $|\alpha\rangle = \hat{D}(\bar{q},\bar{p})|0\rangle$ where $|0\rangle$ is the vacuum state of the harmonic oscillator. The parameter $\alpha = \alpha_x + i\alpha_y$ is defined via the relations $\bar{q} = \sqrt{2\hbar}\alpha_x/\lambda$ and $\bar{p} = \sqrt{2\hbar}\alpha_y\lambda$. The Wigner function of the coherent state $|\alpha\rangle\rangle$ has a Gaussian form

$$W_{|\alpha\rangle}(q,p) = \frac{1}{\sigma_q\sigma_p}\exp\left[-\frac{1}{2\hbar}\frac{(q-\bar{q})^2}{\sigma_q^2} - \frac{1}{2\hbar}\frac{(p-\bar{p})^2}{\sigma_p^2}\right], \quad (6.12)$$

where

$$\sigma_q^2 = \frac{1}{2\lambda^2} \qquad \text{and} \qquad \sigma_p^2 = \frac{\lambda^2}{2}. \quad (6.13)$$

If we assume α to be real, then the Wigner function of the even coherent state reads

$$W_{|\alpha_e\rangle}(q,p) = N_e\left[W_{|\alpha\rangle}(q,p) + W_{|-\alpha\rangle}(q,p) + W_{int}(q,p)\right]; \quad (6.14)$$

where $W_{|\pm\alpha\rangle}(q,p)$ is the WF of coherent states $|\pm\alpha\rangle$. The interference part of the Wigner function (6.14) is given by the relation

$$W_{int}(q,p) = \frac{2}{\sigma_q\sigma_p}\exp\left[-\frac{q^2}{2\hbar\sigma_q^2} - \frac{p^2}{2\hbar\sigma_p^2}\right]\cos\left(\frac{\bar{q}p}{\hbar\sigma_q\sigma_p}\right), \quad (6.15)$$

We plot the Wigner function of the even coherent state in Fig. 6.1. From the figure it is clearly seen that the interference term (6.15) results in oscillations of the Wigner function around the origin of the phase space.

6.2.3 Quantum Homodyne Tomography

The relation (6.9) for the probability distribution $w_{\hat{\rho}}(q)$ of the position operator $\hat{q}$ can be generalized to the case of the distribution of the rotated quadrature operator $\hat{x}_\theta$. This operator is defined as

$$\hat{x}_\theta = \sqrt{\frac{\hbar}{2}} \left[\hat{a} \mathrm{e}^{-i\theta} + \hat{a}^\dagger \mathrm{e}^{i\theta} \right], \tag{6.16}$$

and the corresponding conjugated operator $\hat{x}_{\theta+\pi/2}$, such that $[\hat{x}_\theta, \hat{x}_{\theta+\pi/2}] = i\hbar$, reads

$$\hat{x}_{\theta+\pi/2} = \frac{\sqrt{\hbar}}{i\sqrt{2}} \left[\hat{a} \mathrm{e}^{-i\theta} - \hat{a}^\dagger \mathrm{e}^{i\theta} \right]. \tag{6.17}$$

The position and the momentum operators are related to the operator $\hat{x}_\theta$ as, $\hat{q} = \hat{x}_0$ and $\hat{x}_{\pi/2} = \hat{p}$. The rotation (i.e., the linear homogeneous canonical transformation) given by (6.16) and (6.17) can be performed by the unitary operator $\hat{U}(\theta)$:

$$\hat{U}(\theta) = \exp\left[-i\theta \hat{a}^\dagger \hat{a} \right], \tag{6.18}$$

so that

$$\hat{x}_\theta = \hat{U}^\dagger(\theta) \hat{x}_0 \hat{U}(\theta); \qquad \hat{x}_{\theta+\pi/2} = \hat{U}^\dagger(\theta) \hat{x}_{\pi/2} \hat{U}(\theta). \tag{6.19}$$

Alternatively, in the vector formalism we can rewrite the transformation (6.19) as

$$\begin{pmatrix} \hat{x}_\theta \\ \hat{x}_{\theta+\pi/2} \end{pmatrix} = \mathbf{F} \begin{pmatrix} \hat{q} \\ \hat{p} \end{pmatrix}; \qquad \mathbf{F} = \begin{pmatrix} \cos\theta & \sin\theta \\ -\sin\theta & \cos\theta \end{pmatrix}. \tag{6.20}$$

Eigenvalues x_θ and $x_{\theta+\pi/2}$ of the operators $\hat{x}_\theta$ and $\hat{x}_{\theta+\pi/2}$ can be expressed in terms of the eigenvalues q and p of the position and momentum operators as:

$$\begin{pmatrix} x_\theta \\ x_{\theta+\pi/2} \end{pmatrix} = \mathbf{F} \begin{pmatrix} q \\ p \end{pmatrix}; \qquad \begin{pmatrix} q \\ p \end{pmatrix} = \mathbf{F}^{-1} \begin{pmatrix} x_\theta \\ x_{\theta+\pi/2} \end{pmatrix};$$
$$\mathbf{F}^{-1} = \begin{pmatrix} \cos\theta & -\sin\theta \\ \sin\theta & \cos\theta \end{pmatrix}, \tag{6.21}$$

where the matrix $\mathbf{F}$ is given by (6.20) and $\mathbf{F}^{-1}$ is the corresponding inverse matrix. It has been shown by Ekert and Knight [10] that Wigner functions are transformed under the action of the linear canonical transformation (6.20) as:

$$\begin{aligned} W_{\hat{\rho}}(q,p) &\to W_{\hat{\rho}}(\mathbf{F}^{-1}(x_\theta, x_{\theta+\pi/2})) \\ &= W_{\hat{\rho}}(x_\theta \cos\theta - x_{\theta+\pi/2} \sin\theta; x_\theta \sin\theta + x_{\theta+\pi/2} \cos\theta), \end{aligned} \tag{6.22}$$

which means that the probability distribution $w_{\hat{\rho}}(x_\theta, \theta) = \sqrt{2\pi\hbar}\langle x_\theta|\hat{\rho}|x_\theta\rangle$ can be evaluated as

$$w_{\hat{\rho}}(x_\theta, \theta) = \frac{1}{\sqrt{2\pi\hbar}} \int_{-\infty}^{\infty} dx_{\theta+\pi/2} \times W_{\hat{\rho}}(x_\theta \cos\theta - x_{\theta+\pi/2} \sin\theta; x_\theta \sin\theta + x_{\theta+\pi/2} \cos\theta). \quad (6.23)$$

As shown by Vogel and Risken [11] (see also [12–15]) the knowledge of $w_{\hat{\rho}}(x_\theta, \theta)$ for all values of θ (such that $[0 < \theta \leq \pi]$) is equivalent to the knowledge of the Wigner function itself. This Wigner function can be obtained from the set of distributions $w_{\hat{\rho}}(x_\theta, \theta)$ via the inverse Radon transformation:

$$W_{\hat{\rho}}(q, p) = \frac{1}{(2\pi\hbar)^{3/2}} \int_{-\infty}^{\infty} dx_\theta \int_{-\infty}^{\infty} d\xi\, |\xi| \times \int_0^{\pi} d\theta\, w_{\hat{\rho}}(x_\theta, \theta) \exp\left[\frac{i}{\hbar}\xi(x_\theta - q\cos\theta - p\sin\theta)\right]. \quad (6.24)$$

We stress that the transformation (6.24) is a "deterministic" inverse transformation with the help of which the complete knowledge about the state encoded in the marginal distributions $w_{\hat{\rho}}(x_\theta, \theta)$ is rewritten in a form of the Wigner function.

This reconstruction scheme has been used by Raymer and his coworkers [16,17]; see also chapter by Raymer and Beck of this volume for more details. In their experiments the Wigner functions of a coherent state and a squeezed vacuum state have been reconstructed from tomographic data.

Quantum-state tomography can be applied not only to optical fields but also for reconstruction of other physical systems. In particular, Janicke and Wilkens [18] have suggested that Wigner functions of atomic waves can be tomographically reconstructed. Kurtsiefer et al. [19] have performed experiments in which Wigner functions of matter wave packets have been reconstructed. Yet another example of the tomographic reconstruction is a reconstruction of Wigner functions of vibrational states of trapped atomic ions theoretically described by a number of groups [20] and experimentally measured by Leibfried et al. [21]. Vibrational motional states of molecules have also been reconstructed by this kind of quantum tomography by Dunn et al. [22].

The problem with the inverse Radon transformation is that it does not take into account the possibility of a finite number of measured distributions. As we will show later, in the case of incomplete tomographic data the transformation (6.24) can lead to unphysical reconstructions (e.g. non-positive density operators). In what follows we briefly review a quantum tomography scheme that is based on the sampling via the pattern functions which is equivalent to the inverse Radon transformation.

6.2.4 Quantum Tomography via Pattern Functions

In a sequence of papers D'Ariano et al. [14], Leonhardt et al. [23] and Richter [24] have shown that Wigner functions can be very efficiently reconstructed from tomographic data with the help of the so-called pattern functions. This reconstruction procedure is more efficient than the usual Radon transformation [25]. To be specific, D'Ariano et al. [14] and Kühn et al. [15] have shown that the density matrix ρ_{mn} in the Fock basis can be reconstructed directly from the tomographic data, i.e. from the quadrature-amplitude "histograms" (probabilities), $w(x_\theta, \theta)$ via the so-called *direct sampling method* when

$$\rho_{mn} = \int_0^\pi \int_{-\infty}^\infty w(x_\theta, \theta) F_{mn}(x_\theta, \theta)\, dx_\theta\, d\theta, \tag{6.25}$$

where $F_{mn}(x_\theta, \theta)$ is a set of specific *sampling* functions (see below). Once the density matrix elements are reconstructed with the help of (6.25) then the Wigner function of the corresponding state can be directly obtained using the relation

$$W_{\hat{\rho}}(q,p) = \sum_{m,n} \rho_{mn} W_{|m\rangle\langle n|}(q,p), \tag{6.26}$$

where $W_{|m\rangle\langle n|}(q,p)$ is the Wigner function of the operator $|m\rangle\langle n|$.

A serious problem with the direct sampling method as proposed by D'Ariano et al. [14] is that the sampling functions $F_{mn}(x_\theta, \theta)$ are difficult to compute. Later D'Ariano, Leonhardt and Paul [23, 26] have simplified the expression for the sampling function and have found that it can be expressed as

$$F_{mn}(x_\theta, \theta) = f_{mn}(x_\theta) \exp\left[i(m-n)\theta\right], \tag{6.27}$$

where the so-called *pattern* function "picks up" the pattern in the quadrature histograms (probability distributions) $w_{mn}(x_\theta, \theta)$ that just match the corresponding density-matrix elements. Leonhardt et al. [25] have shown that the pattern function $f_{mn}(x_\theta)$ can be expressed as derivatives

$$f_{mn}(x) = \frac{\partial}{\partial x} g_{mn}(x), \tag{6.28}$$

of functions $g_{mn}(x)$ that are given by the Hilbert transformation

$$g_{mn}(x) = \frac{\mathcal{P}}{\pi} \int_{-\infty}^\infty \frac{\psi_m(\zeta)\psi_n(\zeta)}{x-\zeta} d\zeta, \tag{6.29}$$

where $\mathcal{P}$ stands for the principal value of the integral and $\psi_n(x)$ are the real energy eigenfunctions of the harmonic oscillator, i.e. the normalizable

solutions of the Schrödinger equation

$$\left(-\frac{\hbar^2}{2}\frac{d^2}{dx^2}+\frac{x^2}{2}\right)\psi_n(x)=\hbar(n+1/2)\psi_n(x), \tag{6.30}$$

(we assume $m=\omega=1$). Further details of possible applications and discussion devoted to numerical procedures of the reconstruction of density operators via the direct sampling method can be found in [25].

6.3 Maxent Principle and Observation Levels

The state of a quantum system can always be described by a statistical density operator $\hat{\rho}$. Depending on the system preparation, the density operator represents either a pure quantum state (complete system preparation) or a statistical mixture of pure states (incomplete preparation). The degree of deviation of a statistical mixture from the pure state can be best described by the *uncertainty measure* $\eta[\hat{\rho}]$ (see [27, 28])

$$\eta[\hat{\rho}]=-\operatorname{Tr}(\hat{\rho}\ln\hat{\rho}). \tag{6.31}$$

The uncertainty measure $\eta[\hat{\rho}]$ possesses the following properties:
1. In the eigenrepresentation of the density operator $\hat{\rho}$

$$\hat{\rho}\,|r_m\rangle=r_m|r_m\rangle, \tag{6.32}$$

we can write

$$\eta[\hat{\rho}]=-\sum_m r_m\ln r_m\geq 0, \tag{6.33}$$

where r_m are eigenvalues and $|r_m\rangle$ the eigenstates of $\hat{\rho}$.
2. For uncertainty measure $\eta[\hat{\rho}]$ the following inequality holds:

$$0\leq\eta[\hat{\rho}]\leq\ln N, \tag{6.34}$$

where N denotes the dimension of the Hilbert space of the system and $\eta[\hat{\rho}]$ takes its maximum value when

$$\hat{\rho}=\frac{\hat{1}}{\operatorname{Tr}\hat{1}}=\frac{\hat{1}}{N}\,. \tag{6.35}$$

In this case all pure states in the mixture appear with the same probability equal to $1/N$. If the system is prepared in a pure state then it holds that $\eta[\hat{\rho}]=0$.
3. It can be shown with the help of the Liouville equation

$$\frac{\partial}{\partial t}\hat{\rho}(t)=-\frac{i}{\hbar}[\hat{H},\hat{\rho}(t)], \tag{6.36}$$

that in the case of an isolated system the uncertainty measure is a constant of motion, i.e.,

$$\frac{d\eta(t)}{dt}=0. \tag{6.37}$$

6.3.1 MaxEnt Principle

When instead of the density operator $\hat{\rho}$, expectation values G_ν of a set $\mathcal{O}$ of operators $\hat{G}_\nu$ ($\nu = 1, \ldots, n$) are given, then the uncertainty measure can be determined as well. The set of linearly independent operators is referred to as the *observation level* $\mathcal{O}$ [29,30]. The operators $\hat{G}_\nu$ that belong to a given observation level do not commutate necessarily. A large number of density operators that fulfill the conditions

$$\begin{aligned} \mathrm{Tr}\,\hat{\rho}_{\{\hat{G}\}} &= 1, \\ \mathrm{Tr}\,(\hat{\rho}_{\{\hat{G}\}}\hat{G}_\nu) &= G_\nu\,, \quad \nu = 1, 2, ..., n; \end{aligned} \tag{6.38}$$

can be found for a given set of expectation values $G_\nu = \langle \hat{G}_\nu \rangle$. That is, the conditions (6.38) specify a set $\mathcal{C}$ of density operators, which has to be considered. Each of these density operators $\hat{\rho}_{\{\hat{G}\}}$ can possess a different value of the uncertainty measure $\eta[\hat{\rho}_{\{\hat{G}\}}]$. If we wish to use only the expectation values G_ν of the chosen observation level for determining the density operator, we must select a particular density operator $\hat{\rho}_{\{\hat{G}\}} = \hat{\sigma}_{\{\hat{G}\}}$ in an unbiased manner. According to the Jaynes principle of the Maximum Entropy [29–34] this density operator $\hat{\sigma}_{\{\hat{G}\}}$ must be the one that has the largest uncertainty measure

$$\eta_{\max} \equiv \max\left\{\eta[\hat{\sigma}_{\{\hat{G}\}}]\right\} \tag{6.39}$$

and simultaneously fulfills constraints (6.38). As a consequence of (6.39) the following fundamental inequality holds

$$\eta[\hat{\sigma}_{\{\hat{G}\}}] = -\mathrm{Tr}(\hat{\sigma}_{\{\hat{G}\}} \ln \hat{\sigma}_{\{\hat{G}\}}) \geq \eta[\hat{\rho}_{\{\hat{G}\}}] = -\mathrm{Tr}(\hat{\rho}_{\{\hat{G}\}} \ln \hat{\rho}_{\{\hat{G}\}}) \tag{6.40}$$

for all possible $\hat{\rho}_{\{\hat{G}\}}$ that fulfill (6.38). The variation determining the maximum of $\eta[\hat{\sigma}_{\{\hat{G}\}}]$ under the conditions (6.38) leads to a generalized canonical density operator [29–31,33]

$$\hat{\sigma}_{\{\hat{G}\}} = \frac{1}{Z_{\{\hat{G}\}}} \exp\,(-\sum_\nu \lambda_\nu \hat{G}_\nu); \tag{6.41}$$

$$Z_{\{\hat{G}\}}(\lambda_1, ..., \lambda_n) = \mathrm{Tr}[\exp(-\sum_\nu \lambda_\nu \hat{G}_\nu)], \tag{6.42}$$

where λ_n are the Lagrange multipliers and $Z_{\{\hat{G}\}}(\lambda_1, \ldots \lambda_n)$ is the generalized partition function. By using the derivatives of the partition function we obtain the expectation values G_ν as

$$G_\nu = \mathrm{Tr}(\hat{\sigma}_{\{\hat{G}\}}\hat{G}_\nu) = -\frac{\partial}{\partial \lambda_\nu} \ln Z_{\{\hat{G}\}}(\lambda_1, ..., \lambda_n), \tag{6.43}$$

where in the case of noncommuting operators the following relation has to be used

$$\frac{\partial}{\partial a}\exp[-\hat{X}(a)] = \exp[-\hat{X}(a)]\int_0^1 \exp[\mu\hat{X}(a)]\frac{\partial\hat{X}(a)}{\partial a}\exp[-\mu\hat{X}(a)]\,d\mu. \quad (6.44)$$

By using (6.43) the Lagrange multipliers can, in principle, be expressed as functions of the expectation values

$$\lambda_\nu = \lambda_\nu(G_1, ..., G_n). \quad (6.45)$$

We note that (6.43) for Lagrange multipliers do not always have solutions which lead to physical results, which means that in these cases states of quantum systems cannot be reconstructed on a given observation level.

The maximum uncertainty measure regarding an observation level $\mathcal{O}_{\{\hat{G}\}}$ will be referred to as the entropy $S_{\{\hat{G}\}}$

$$S_{\{\hat{G}\}} \equiv \eta_{\max} = -\mathrm{Tr}(\hat{\sigma}_{\{\hat{G}\}}\ln\hat{\sigma}_{\{\hat{G}\}}). \quad (6.46)$$

This means that to different observation levels different entropies are related. By inserting $\sigma_{\{\hat{G}\}}$ [cf. (6.41)] into (6.46), we obtain the following expression for the entropy

$$S_{\{\hat{G}\}} = \ln Z_{\{\hat{G}\}} + \sum_\nu \lambda_\nu G_\nu. \quad (6.47)$$

By making use of (6.45), the parameters λ_ν in the above equation can be expressed as functions of the expectation values G_ν and this leads to a new expression for the entropy

$$S_{\{\hat{G}\}} = S(G_1, ..., G_n). \quad (6.48)$$

We note that using the expression

$$dS_{\{\hat{G}\}} = \sum_\nu \lambda_\nu dG_\nu, \quad (6.49)$$

which follows from (6.43) and (6.47) the following relation can be obtained

$$\lambda_\nu = \frac{\partial}{\partial G_\nu}S(G_1, ..., G_n). \quad (6.50)$$

6.3.2 Linear Transformations Within an Observation Level

An observation level can be defined either by a set of linearly independent operators $\{\hat{G}_\nu\}$, or by a set of independent linear combinations of the same operators

$$\hat{G}'_\mu = \sum_\nu c_{\mu\nu}\hat{G}_\nu. \tag{6.51}$$

Therefore, $\hat{\sigma}$ and S are invariant under a linear transformation:

$$\hat{\sigma}'_{\{\hat{G}'\}} = \frac{\exp(-\sum_\mu \lambda'_\mu \hat{G}'_\mu)}{\mathrm{Tr}\exp(-\sum_\mu \lambda'_\mu \hat{G}'_\mu)} = \hat{\sigma}_{\{\hat{G}\}}. \tag{6.52}$$

As a result, the Lagrange multipliers transform contravariantly to (6.51), i.e.,

$$\lambda'_\mu = \sum_\nu c'_{\mu\nu}\lambda_\nu\,, \tag{6.53}$$

$$\sum_\mu c'_{\nu\mu}c_{\mu\rho} = \delta_{\nu\rho}\,. \tag{6.54}$$

6.3.3 Extension and Reduction of the Observation Level

If an observation level $\mathcal{O}_{\{\hat{G}\}} \equiv \hat{G}_1, \ldots, \hat{G}_n$ is extended by including further operators $\hat{M}_1, \ldots, \hat{M}_l$, then additional expectation values $M_1 = \langle\hat{M}_1\rangle, \ldots, M_l = \langle\hat{M}_l\rangle$ can only increase the amount of available information about the state of the system. This procedure is called the *extension* of the observation level (from $\mathcal{O}_{\{\hat{G}\}}$ to $\mathcal{O}_{\{\hat{G},\hat{M}\}}$) and is associated with a decrease of the entropy. More precisely, the entropy $S_{\{\hat{G},\hat{M}\}}$ of the extended observation level $\mathcal{O}_{\{\hat{G},\hat{M}\}}$ can be only smaller or equal to the entropy $S_{\{\hat{G}\}}$ of the original observation level $\mathcal{O}_{\{\hat{G}\}}$,

$$S_{\{\hat{G},\hat{M}\}} \leq S_{\{\hat{G}\}}\,. \tag{6.55}$$

The generalized canonical density operator of the observation level $\mathcal{O}_{\{\hat{G},\hat{M}\}}$

$$\hat{\sigma}_{\{\hat{G},\hat{M}\}} = \frac{1}{Z_{\{\hat{G},\hat{M}\}}} \exp\left(-\sum_{\nu=1}^{n}\lambda_\nu\hat{G}_\nu - \sum_{\mu=1}^{l}\kappa_\mu\hat{M}_\mu\right), \tag{6.56}$$

with

$$Z_{\{\hat{G},\hat{M}\}} = \mathrm{Tr}\left[\exp\left(-\sum_{\nu=1}^{n}\lambda_\nu\hat{G}_\nu - \sum_{\mu=1}^{l}\kappa_\mu\hat{M}_\mu\right)\right], \tag{6.57}$$

belongs to the set of density operators $\hat{\rho}_{\{\hat{G}\}}$ fulfilling (6.38). Therefore, (6.56) is a special case of (6.41). Analogously to (6.43) and (6.45), the Lagrange

multipliers can be expressed by functions of the expectation values

$$\lambda_\nu = \lambda_\nu(G_1, ..., G_n, M_1, ..., M_l),$$
$$\kappa_\mu = \kappa_\mu(G_1, ..., G_n, M_1, ..., M_l). \tag{6.58}$$

The sign of equality in (6.55) holds only for $\kappa_\mu = 0$. In this special case the expectation values M_μ are functions of the expectation values G_ν. The measurement of observables $\hat{M}_\mu$ does not increase information about the system. Consequently, $\hat{\rho}_{\{\hat{G},\hat{M}\}} = \hat{\rho}_{\{\hat{G}\}}$ and $S_{\{\hat{G},\hat{M}\}} = S_{\{\hat{G}\}}$.

We can also consider a *reduction of the observation level* if we decrease the number of independent observables that are measured, e.g., $\mathcal{O}_{\{\hat{G},\hat{M}\}} \to \mathcal{O}_{\{\hat{G}\}}$. This reduction is accompanied by an increase of the entropy due to the decrease of the information available about the system.

6.3.4 Wigner Functions on Different Observation Levels

With the help of a generalized canonical density operator $\hat{\sigma}_{\{\hat{G}\}}$ we define the Wigner function in the ξ phase space at the corresponding observation level as

$$W_{\{\hat{G}\}}(\xi) = \frac{1}{\pi} \int d^2\eta \mathrm{Tr}\left[\hat{D}(\eta)\hat{\sigma}_{\{\hat{G}\}}\right] \exp\left(\xi\eta^* - \xi^*\eta\right). \tag{6.59}$$

Analogous expression can be found for the Wigner function in the (q, p) phase space.

6.3.5 MaxEnt Principle and Laws of Physics

It has been pointed out by Jaynes in his Brandeis lectures [1] that there is a strong formal resemblance between the MaxEnt formalism and the rules of calculations in statistical mechanics and thermodynamics. Simultaneously he has emphasized that the MaxEnt principle "has nothing to do with the laws of physics"[3]. To be more specific it is worth citing a paragraph from the Jaynes' Brandeis lectures (see p. 183 of these lectures [1]): "Conventional quantum theory has provided an answer to the problem of setting up initial state descriptions only in the limiting case where measurements of a "complete set of commuting observables" have been made, the density matrix $\hat{\rho}(0)$ then reducing to the projection operator onto a pure state $\psi(0)$ which is the appropriate simultaneous eigenstate of all measured quantities. But there is almost no experimental situation in which we really have all this information, and before we have a theory able to treat actual experimental situations, existing quantum theory must be supplemented with some principle that tells us

[3] In fact, this is the reason why the MaxEnt principle is applicable in so many fields of human activities, for instance we can mention economy or sociology (for more details see the book by Kapur and Kevasan [32]).

how to translate, or encode, the results of measurements into a definite state description $\hat{\rho}(0)$. Note that the problem is not to find $\hat{\rho}(0)$ which correctly describes "true physical situation". That is unknown, and always remains so, because of incomplete information. In order to have a usable theory we must ask the much more modest question: *What* $\hat{\rho}(0)$ *best describes our state of knowledge about the physical situation?*".

In other words, the MaxEnt principle is *the most conservative assignment in the sense that it does not permit one to draw any conclusions not warranted by the data*. From this point of view the MaxEnt principle has a very close relation (or can be understood as the generalization) of the Laplace's principle of *indifference* [35] which states that where nothing is known one should choose a constant valued function to reflect this ignorance. Then it is just a question of how to quantify a degree of this ignorance. If we choose an entropy to quantify the ignorance, then the relation between the Laplace's indifference principle and the Jaynes principle of the Maximum Entropy is transparent, i.e. for a constant-valued probability distribution the entropy takes its maximum value.

We can conclude that a measurement itself is a physical process and is governed by the laws of physics. On the other hand formal procedures by means of which we reconstruct information about the system from the measured data are based on certain principles that cannot be directly expressed in terms of the physical laws.

6.3.6 Quantum Tomography via MaxEnt Principle

The probability density distribution $w_{\hat{\rho}}(x_\theta)$ [see (6.23)] for rotated quadratures $\hat{x}_\theta$ can be represented as a result of the measurement of the continuous set of projectors $|x_\theta\rangle\langle x_\theta|$. Based on the measurement of the distributions $w_{\hat{\rho}}(x_\theta)$ for all values of $\theta \in [0, \pi]$ we can formally "reconstruct" the density operator according to the formula

$$\hat{\rho}_{_{ME}} = \frac{1}{Z_0} \exp\left[- \int_0^\pi d\theta \int_{-\infty}^{\infty} dx_\theta \, |x_\theta\rangle\langle x_\theta| \lambda(x_\theta) \right], \tag{6.60}$$

where the Lagrange multipliers $\lambda(x_\theta)$ are given by an infinite set of equations

$$w_{\hat{\rho}}(x_\theta) = \sqrt{2\pi\hbar} \langle x_\theta | \hat{\rho}_{_{ME}} | x_\theta \rangle; \qquad \forall x_\theta \in (-\infty, \infty). \tag{6.61}$$

If the distributions $w_{\hat{\rho}}(x_\theta)$ are measured for all values of x_θ and all angles θ then the density operator $\hat{\rho}_{_{ME}}$ is reconstructed precisely and is equal to the density operator obtained with the help of the inverse Radon transformation (or with the help of the pattern functions).

In practical experimental situations (see the experiments by Raymer et al. [16] and by Mlynek et al. [19]) it is impossible to measure the distributions $w_{\hat{\rho}}(x_\theta)$ for all values of x_θ and all angles θ. What is measured are distributions (histograms) for finite number N_θ quadrature angles θ and the

finite number N_x of bins for quadrature operators. This means that practical experiments are associated with an observation level specified by a finite number of observables

$$\hat{Q}_{nm} = |x_{\theta_m}^{(n)}\rangle\langle x_{\theta_m}^{(n)}| \tag{6.62}$$

with number of quadrature angles equal to N_θ and the number of bins for each quadrature equal to N_x. These observables in the Fock basis can be represented as

$$\left(\hat{Q}_{nm}\right)_{k_1,k_2} = \psi_{k_1}^{\star}(x_n)\psi_{k_2}(x_n)\exp[i\theta_m(k_1-k_2)], \tag{6.63}$$

where θ_m is the quadrature phase, x_n is eigenvalue of the quadrature operator and $\psi_k(x)$ is the wave function of the kth energy eigenstate (Fock state) of the harmonic oscillator. We can therefore assume that from the measurement of the observables $\hat{Q}_{nm}$ the mean values $\overline{Q}_{nm}$ are determined (these mean values correspond to "discretized" quadrature distributions). In addition, it is usually the case that the mean photon number of the state is known (measured) as well.

The operators $\hat{Q}_{nm}$ together with $\hat{n}$ form a specific observation level corresponding to the incomplete tomographic measurement. In this case we can express the generalized canonical density operator in the form

$$\hat{\rho}_{ME} = \frac{1}{Z}\exp\left(-\lambda_0\hat{n} - \sum_{n=1}^{N_x}\sum_{m=1}^{N_\theta}\lambda_{n,m}|x_{\theta_m}^{(n)}\rangle\langle x_{\theta_m}^{(n)}|\right) \tag{6.64}$$

The knowledge of the mean photon number is essential for the *MaxEnt* reconstruction because it formally regularizes the *MaxEnt* reconstruction scheme (the generalized partition function is finite in this case).

6.4 Numerical Implementation

Let us summarize what is supposed to be known as a result of the measurement - these are the measured mean values $\overline{Q}_{nm}$ and $\overline{n}$ of the observables $\hat{Q}_{nm}$ and $\hat{n}$, respectively. Further, the experimental setup gives us the numbers N_θ and N_x as well as the size Δx of quadrature bins. These last two numbers specify the range of measured quadratures $-N_x\Delta x/2 \leq x \leq N_x\Delta x/2$.

In addition to these "experimental" parameters we have to specify also the dimensionality N_{max} of the Hilbert space in which we reconstruct the density operator. In the case of the *MaxEnt* reconstruction N_{max} has to be chosen so that the "truncation" of the Hilbert space does not affect the reconstruction of the state of original light field (i.e. $N_{max} \gg \overline{n}$ so that the reconstructed state "fits" into the truncated Hilbert space).

To perform the reconstruction we have to determine the Lagrange multipliers $\lambda_{n,m}$ in the expression for the generalized canonical density operator (6.64). These multipliers are given by the constraints (6.38) and numerically can be determined via the minimization of a deviation function ΔQ with respect to the measured mean photon number $\bar{n}$ and the set of histograms $\bar{Q}_{nm} = \mathrm{Tr}\{\hat{\rho}\hat{Q}_{nm}\}$:

$$\Delta Q = (\bar{n} - \mathrm{Tr}\{\hat{\rho}_{ME}\hat{n}\})^2 + \sum_{n,m=1}^{N_\theta, N_x} \left(\bar{Q}_{nm} - \mathrm{Tr}\left\{\hat{\rho}_{ME}\hat{Q}_{nm}\right\}\right)^2 . \quad (6.65)$$

The trace is performed within the truncated Hilbert space specified by the parameter N_{max}. When $\Delta Q = 0$ the Lagrange multipliers are determined precisely and the reconstructed density operator $\hat{\rho}_{ME}$ *ideally* satisfies the mean values of measured observables.

In order to find the minimal value of the function ΔQ and to determine the Lagrange multipliers we utilize the Levenberg-Marquardt algorithm with a finite difference Jacobian (see a standard routine from the IMSL library, Visual Numerics, Inc., `http://www.vni.com`).

Once the Lagrange multipliers are specified, then, using the expression for the generalized canonical density operator (6.64), we can plot the corresponding Wigner function. The fidelity of the reconstruction is given by three parameters. Firstly, it is the minimal value of the function ΔQ that determines the deviation between the measured mean values of the observables and the corresponding mean values evaluated from the reconstructed density operator. Secondly, if it is a priori known that the measured system is prepared in a pure state then the von Neumann entropy S of the density operator $\hat{\rho}_{ME}$ is a measure of the fidelity of the reconstruction. Specifically, if the entropy is equal to zero then the pure state is perfectly reconstructed. Thirdly, if we want to test the reconstruction scheme we can compare the reconstructed density operator with the known original $\hat{\rho}$. In this case we can use the measure

$$\Delta\rho = \sum_{m,n}^{N_x, N_\theta} |(\hat{\rho})_{mn} - (\hat{\rho}_{ME})_{mn}|^2 . \quad (6.66)$$

Let us test the *MaxEnt* reconstruction scheme and assume the mean values of the observables $\hat{Q}_{mn}$ to be given by the even coherent state (6.11) with the real amplitude $\alpha = 2$ (we plot the Wigner function of this state in Fig. 6.2a).

Let us further assume just two quadrature angles $N_\theta = 2$ corresponding to the measurement of the position and the momentum of the harmonic oscillator. The total number of bins for each quadrature is taken to be $N_x = 40$ with the size of the bin equal to $\Delta x = 0.2$ (we assume $\hbar = 1$), which corresponds to the measurement of the quadrature distributions on the interval $\langle -4, 4\rangle$. For the given mean photon number ($\bar{n} \simeq 4$) it is enough to consider the Hilbert space of the dimension $N_{max} = 20$. The even coherent state with

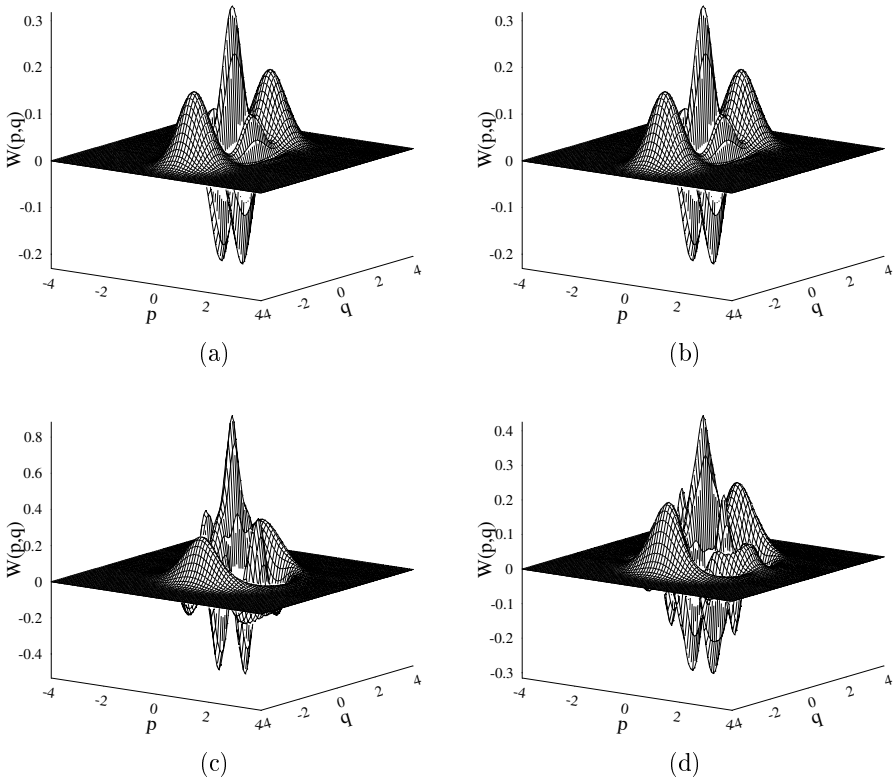

Fig. 6.2. (a) The Wigner function of the even coherent state with $\alpha = 2$. (b) Reconstruction of the Wigner function via the *MaxEnt* principle from two marginal distributions ($N_\theta = 2$) for the position and momentum. The measured marginal distributions are divided into $N_x = 40$ bins of the width $\Delta x = 0.2$ covering the interval $\langle -4, 4\rangle$. The fidelity of the reconstruction is $\Delta Q = 5.4 \times 10^{-12}$ and $\Delta\rho = 1.0 \times 10^{-8}$, the corresponding entropy is $S \approx 10^{-6}$. (c) Optical tomography via the direct sampling using pattern functions with $N_\theta = 2$ and with an artificial truncation at $N_{max} = 4$. This value of N_{max} is chosen such that the deviation ΔQ is minimized. In this case $\Delta Q \simeq 9.17$ and $\Delta\rho \simeq 3.7$. The reconstructed Wigner function is unphysical because the corresponding density operator has negative probabilities for odd Fock states ($P_1 \approx -0.35$, $P_3 \approx -0.54$). (d) The result of the tomography can be improved when the number of quadratures is larger. For $N_\theta = 4$ and the truncation at $N_{max} = 6$ we can improve the fidelity of the reconstruction ($\Delta Q \simeq 1.33$ and $\Delta\rho = 0.51$) but it is still unphysical because $P_1 \approx -0.1$.

$\alpha = 2$ can be very well approximated as a superposition of even number states up to $n = 8$ (the higher number states are occupied with 1% probability), so $N_{max} = 20$ is a very good truncation.

With these values of the parameters we have performed the reconstruction of the state via the *MaxEnt* principle. Using the minimization procedure we have achieved the deviation with respect to the "experimental" data $\Delta Q =$

5.4×10^{-12}. The difference between the reconstructed density operator and the original measured in terms of (6.66) in this particular case is $\Delta\rho = 1.0 \times 10^{-10}$. We see that the reconstruction is indeed very precise even for a very small number of experimental data. A high quality of the reconstruction is indicated by the corresponding value of the von Neumann entropy $S \approx 10^{-6}$. We plot the reconstructed Wigner function in Fig. 6.2b. From this figure we see that the reconstruction and the original are essentially identical. We also note that the quality of the reconstruction practically does not depend on the choice of N_{max} when this is larger than some minimal value related to $\bar{n}$ (in our case for $N_{max} > 12$ the reconstruction is almost perfect but even for $N_{max} = 8$ the fidelity is very high).

In order to illustrate the *MaxEnt* reconstruction scheme for statistical mixtures we will consider briefly a statistical mixture described by the density operator

$$\hat{\rho} = \frac{1}{2}|\alpha\rangle\langle\langle\alpha| + \frac{1}{2}|-\alpha\rangle\langle\langle -\alpha| \tag{6.67}$$

with the real amplitude $\alpha = 2$. The Wigner function of this state is plotted in Fig. 6.3a. In the Fig. 6.3b we plot the reconstructed Wigner function under the same conditions as the Fig. 6.2b, i.e. $N_\theta = 2$, $N_x = 40$, $\Delta x = 0.2$ and $N_{max} = 20$. The two measured quadratures are the position and the momentum. We see from the figure that the reconstruction is almost perfect. For this reconstruction we have $\Delta Q = 1.4 \times 10^{-8}$ and $\Delta\rho = 1.1 \times 10^{-8}$. The corresponding entropy $S = 0.694$ is close to $\ln 2$.

Here we note that the size of the bin Δx does not play a significant role in the reconstruction via the *MaxEnt* principle. We will discuss this issue in more detail below, but now we concentrate our attention on the role of the number N_θ of quadrature angles.

6.4.1 Minimal Number of Measured Quadratures

The two quadratures $\hat{q} = \hat{x}_{\theta=0}$ and $\hat{p} = \hat{x}_{\theta=\pi/2}$ are sufficient for a reconstruction of the even coherent state when α is real (this corresponds to specific a priori information about the state). If we consider the most general case, when α is complex, then the reconstruction based on the measurement of just two quadratures is not very good (in what follows, instead of choosing the complex α we will use correspondingly rotated quadratures).

Firstly, let us consider a reconstruction of the even coherent state with the real amplitude α based on the measurement of two rotated quadratures which are not mutually orthogonal (see Fig. 6.4). In particular, let us assume $\hat{x}_{\theta=0}$ and $\hat{x}_{\theta=\pi/8}$. Other settings are the same as in Fig 6.2b. We plot the reconstructed Wigner function in Fig. 6.4a.

It is very similar to the Wigner function of the statistical mixture (which is also indicated by the value of the corresponding von Neumann entropy close to $\ln 2$). The reason is that the type of the measurement considered in the

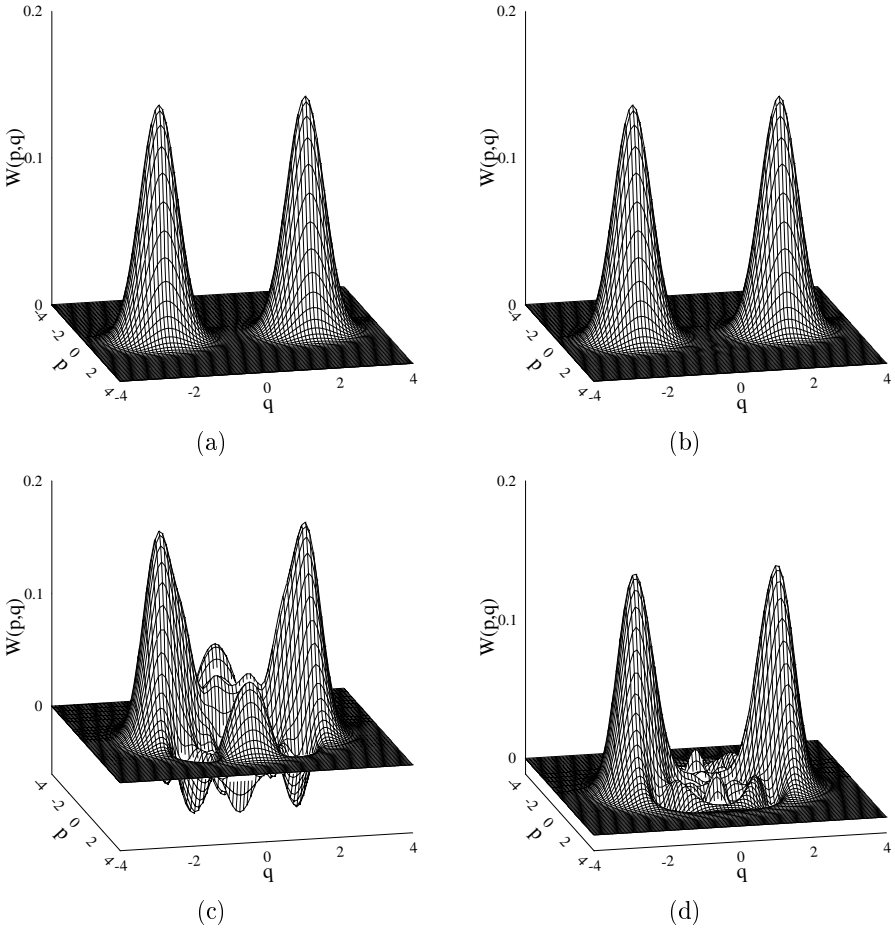

Fig. 6.3. (a) The Wigner function of the mixture of two coherent states with $\alpha = \pm 2$. (b) The reconstruction of the Wigner function via the *MaxEnt* principle based on the measurement of marginal distributions for the position and the momentum ($N_\theta = 2$). The measured marginal distributions are divided into $N_x = 40$ bins of width $\Delta x = 0.2$ covering the interval $\langle -4, 4\rangle$. The fidelity of the reconstruction is $\Delta Q = 1.4 \times 10^{-8}$ and $\Delta\rho = 1.1 \times 10^{-8}$, with entropy $S = 0.694$. (c) The tomography via pattern functions with $N_\theta = 4$ and $N_{max} = 8$ for which the minimum deviation $\Delta Q = 0.71$ is obtained. The fidelity of the reconstruction is $\Delta\rho = 0.17$. The reconstructed density operator is unphysical. (d) For the larger number of quadratures $N_\theta = 8$ with $N_{max} = 8$ we obtain $\Delta Q = 0.13$ and $\Delta\rho = 0.023$. The reconstructed Wigner function still exhibits some fictitious interference structure.

example does not provide us with enough information about the interference pattern in the phase space (the two measured quadratures are "too" close).

Our next example is the case when the two measured quadratures are mutually orthogonal, but are rotated with respect to the position and the

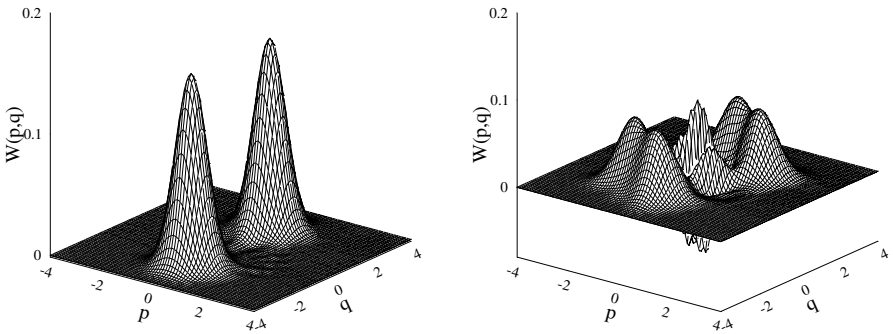

Fig. 6.4. The Wigner function of the even coherent state $\alpha = 2$ reconstructed via *MaxEnt* principle from two particular marginal distributions ($N_\theta = 2$). In (a) we consider two rotated quadratures for $\theta = 0$ and $\theta = \pi/8$. The reconstruction leads to a statistical mixture of two coherent states. The fidelity of the reconstruction is $\Delta Q \approx \times 10^{-6}$, $\Delta\rho = 0.49$, and the entropy is $S = 0.7$. (b) The choice of "measurement angles" $\theta = \pi/8, \pi/2 + \pi/8$ leads to a mixture with $\Delta Q \approx \times 10^{-7}$, $\Delta\rho = 0.60$, and the entropy is $S = 1.31$. Other settings (the number of bins and their width) are the same as in Fig. 6.2.

momentum. Specifically, $\hat{x}_{\theta=\pi/8}$ and $\hat{x}_{\theta=\pi/2+\pi/8}$ and other settings are the same as in Fig 6.2b. We plot the reconstructed Wigner function in Fig. 6.4b. In this Wigner function we see some interference pattern but the information from the measurement does not allow us to perform a reliable reconstruction ($\Delta Q \approx 10^{-7}$, $\Delta\rho = 0.60$, and $S = 1.31$). We can observe some "fictitious" peaks in the reconstructed Wigner function.

To improve the fidelity of the reconstruction we have to consider larger numbers of the rotated quadratures. In fact, it is our empirical experience that three rotated quadratures ($N_\theta = 3$) are always sufficient to perform a very reliable *MaxEnt* reconstruction of an arbitrary unknown state. We have not found yet a rigorous proof for this empirical observation.

6.4.2 Comparison with the Reconstruction via Direct Sampling

It has been shown by Leonhardt et al. [25] that for a reliable reconstruction via direct sampling with the help of the pattern functions two conditions have to be satisfied:

$$\begin{aligned} &N_\theta = N_{max} \\ &\Delta x < \pi/2\sqrt{2N_{max}+1}. \end{aligned} \tag{6.68}$$

This means that the truncation of the Hilbert space in which the reconstructed density operator is defined specifies how many quadrature angles have to be considered as well as it puts some restriction on the size of the bin.

The Role of N_θ

We start with the analysis of the first condition. In our case of the even coherent state with $\alpha = 2$ we have to consider at least $N_{max} = 8$. Consequently, following Leonhardt we would have to consider a measurement of $N_\theta = 8$ quadratures. In this case the precision of reconstruction is $\Delta Q = 0.13$ and $\Delta\rho = 0.03$ which is reasonable, but much smaller than in the case of the *MaxEnt* reconstruction. It is important to remember that any deviation of N_θ from N_{max} causes a dramatic deterioration of the reconstruction scheme (for more details see [25, 36]). In particular, for $N_{max} > N_\theta$ higher "ghost" Fock states appear in the reconstructed density matrix. This effect of aliasing (see [36]) is caused by the fact that in the sampling method the matrix elements ρ_{mn} with $(m-n)\mathrm{mod}N_\theta$ cannot be distinguished.

To see the effect of an insufficient number of phases for the sampling via pattern functions we plot in Fig. 6.2 the results for $N_\theta = 2$ [see (c)] and $N_\theta = 4$ [see (d)] marginal distributions. In both cases we chose N_{max} such that the parameter ΔQ (deviation from the measured data) is minimized. In particular, for $N_\theta = 2$ using the numerical search we have found that ΔQ is minimized for $N_{max} = 4$ when $\Delta Q = 9.17$ and $\Delta\rho = 3.7$. However, the reconstructed density operator is unphysical – we obtain *negative* probabilities of odd Fock states: $P_1 = -0.35$, $P_3 = -0.54$. The corresponding Wigner function is plotted in Fig. 6.2c. Analogously, for $N_\theta = 4$ we have found the optimal truncation to be $N_{max} = 6$. In this case $\Delta Q = 1.33$ and $\Delta\rho = 0.51$. The fidelity of the reconstruction is now better, but it still gives us an unphysical result with $P_1 = -0.1$ (the corresponding Wigner function is plotted in Fig. 6.2d). We have checked that higher values of N_{max} significantly deteriorate the quality of reconstructions. Comparing the sampling method with the result of the *MaxEnt* approach we see the great advantage of the latter for a small number of quadrature phases.

Analogous results are obtained also for statistical mixtures (see Fig. 6.3). Specific values for the fidelities of the reconstruction are given in the figure caption.

The Role of N_x

In addition to the required resolution of bins, i.e. $\Delta x < \pi/2\sqrt{2N_{max}+1}$, the sampling via pattern functions is also very sensitive with respect to the size of the interval on which the marginals are measured. To apply the sampling via pattern functions marginal distributions have been measured on the whole interval where they take non-zero values. The importance of the distribution "tails" of the marginals can be illustrated on the example of the even coherent state. Let us consider the size of the bin (i.e. the resolution) to be $\Delta x = 0.2$ and let us change the values of N_x.

In Fig. 6.5 we plot the reconstructed Wigner functions which are obtained from the incomplete marginal distributions via the *MaxEnt* [(a)-(b)] and via the sampling [(c)-(f)] reconstruction schemes.

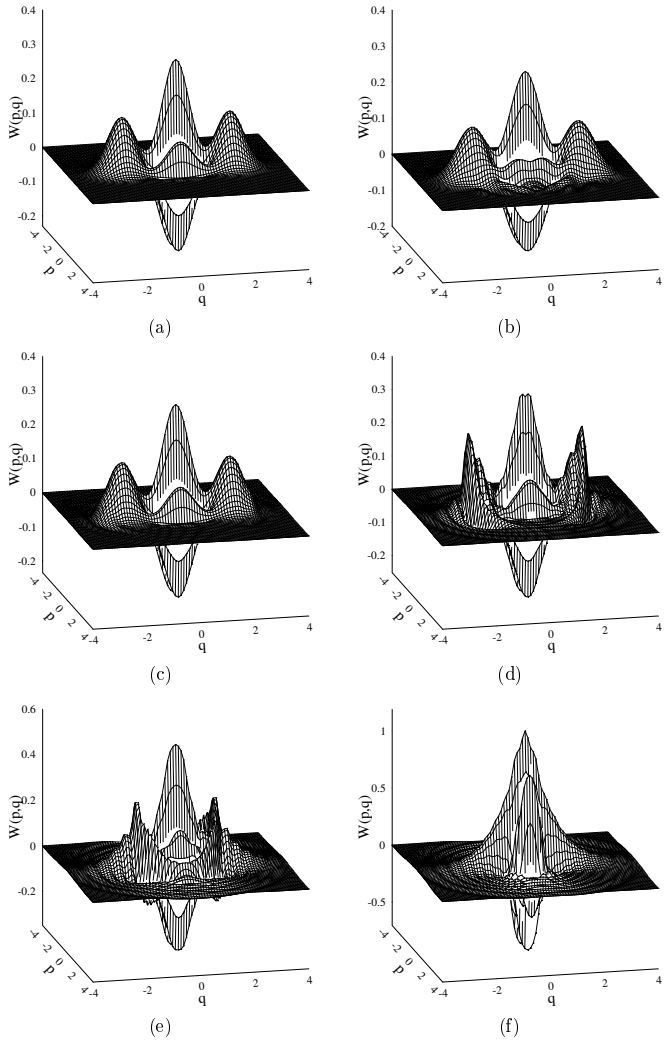

Fig. 6.5. The reconstruction of the Wigner function of the even coherent state with $\alpha = 2$. (a) The reconstruction via the *MaxEnt* principle with two marginal distributions ($N_\theta = 2$) for the position and the momentum. The "measured" marginal distributions are divided into $N_x = 20$ bins of width $\Delta x = 0.2$ covering the interval $\langle -2, 2\rangle$. The fidelity of the reconstruction is $\Delta Q = 2 \times 10^{-15}$ and $\Delta\rho = 2 \times 10^{-10}$ which is comparable with Fig. 6.2b (where $N_x = 40$ corresponding to $x \in \langle -4, 4\rangle$). (b) This is the same example as (a) except $N_x = 10$, i.e. $x \in \langle -1, 1\rangle$. The quality of the reconstruction decreases to $\Delta Q = 3\times 10^{-15}$ and $\Delta\rho = 0.029$. (c)-(f) Reconstruction via pattern functions with $N_\theta = 20$ and $N_{max} = 20$. The marginals are taken within the intervals (c) $\langle -4, 4\rangle$ [$\Delta Q = 0.05$, $\Delta\rho = 0.002$]; (d) $\langle -3, 3\rangle$ [$\Delta Q = 0.88$, $\Delta\rho = 0.154$]; (e) $\langle -2, 2\rangle$ [$\Delta Q = 8.6$, $\Delta\rho = 1.01$]; (f) $\langle -1, 1\rangle$ [$\Delta Q = 47.7$, $\Delta\rho = 5.82$]. We see that the shorter the interval on which the quadrature distribution is measured the less reliable the reconstruction is.

In Fig. 6.5a we plot the reconstruction via the *MaxEnt* principle with two marginal distributions ($N_\theta = 2$). The "measured" marginal distributions are divided into $N_x = 20$ bins of width $\Delta x = 0.2$ covering the interval $\langle -2, 2\rangle$. The quality of the reconstruction is $\Delta Q = 2 \times 10^{-15}$, $\Delta\rho = 2 \times 10^{-10}$, and $S \approx 10^{-8}$ which is comparable with Fig. 6.2b when $N_x = 40$ and $x \in \langle -4, 4\rangle$. We see that even though the interval on which the marginal distributions are measured is shorter by the factor two the fidelity of reconstruction is not affected. In Fig. 6.5b we plot the reconstructed Wigner function under the same conditions except $N_x = 10$, i.e. $x \in \langle -1, 1\rangle$. The quality of the reconstruction decreases to $\Delta Q = 3 \times 10^{-15}$, $\Delta\rho = 0.029$, and $S = 0.20$, but still is rather reliable.

In Figs. 6.5c-f we present results of the reconstruction via direct sampling. We assume $N_\theta = 20$ and $N_{max} = 20$. That is, we consider significantly more data than in the previous two cases. Nevertheless, results of the reconstruction are much worse. Specifically, let us assume the marginal distributions to be taken within the intervals (c) $\langle -4, 4\rangle$ which results in the reconstruction with the fidelity $\Delta Q = 0.05$ and $\Delta\rho = 0.002$. Analogously, (d) $\langle -3, 3\rangle$ with $\Delta Q = 0.88$, $\Delta\rho = 0.154$; (e) $\langle -2, 2\rangle$ with $\Delta Q = 8.6$, $\Delta\rho = 1.01$; (f) $\langle -1, 1\rangle$ with $\Delta Q = 47.7$, $\Delta\rho = 5.82$. We conclude that the shorter the interval on which the quadrature distribution is measured the less reliable the reconstruction is. From Fig. 6.5 it is seen that the sampling via pattern functions can reconstruct only a structure within a measured region of the phase space.

From above we can conclude, that for a reliable use of the reconstruction via the direct sampling we have to measure a sufficient number of quadrature distributions ($N_\theta = N_{max}$) on the whole interval of x. On the contrary, with the *MaxEnt* approach we need just a small number of quadrature distributions and the interval on which the distributions are measured can be rather small. We have also analyzed the situation when the distributions are measured on the interval which is not symmetric with respect to the origin of the phase space. In this case the *MaxEnt* scheme works very reliably while the direct sampling fails completely.

The *MaxEnt* reconstruction scheme can be applied for various quantum systems. In particular, in what follows we will analyze how vibrational states of trapped neutral atoms can be reconstructed.

6.5 Reconstruction of Motional States of Neutral Atoms

In atomic optics a highly coherent control of motional degrees of freedom has been achieved for neutral atoms [37,38]. In order to verify the degree (fidelity) of coherent control over motional degrees of freedom of neutral atoms one can consider a reconstruction of their motional states from measured data. In what follows we will perform this type of analysis.

Recently, experimental manipulations of motional quantum states of neutral atoms have been reported by the group of C. Salomon in Paris [37, 38].

Cold Cs atoms can be cooled into specific quantum states of a far detuned 1D optical lattice. The optical lattice is induced by the interference of two laser beams. Along the vertical z axis a periodic potential of "harmonic" microwells is produced with a period of 665 nm and with an amplitude of about 0.2 μK [38]. The vertical oscillation frequency in a microwell at the center of the trap is $\omega_z/2\pi = 85$ kHz. The corresponding ground state has the rms size $\Delta z_0 = \sqrt{\hbar/2m\omega_z} \approx 21$ nm and $\Delta p_0/m = \sqrt{\hbar\omega_z/2m} \approx 11$ mm/s is its rms velocity width. The trapped cloud of neutral Cs atoms has a nearly Gaussian shape with a vertical rms size $\Delta\xi_0 = 53$ μm. With the help of deterministic manipulations the neutral atoms can be prepared in non-classical 1D motional states along the vertical axis such as squeezed states, number states, or specific superpositions of number states [38]. The measurement of the prepared quantum state $\hat{\rho}$ is performed as follows: The system is evolved within the harmonic potential during the time τ. Then the lasers are turned off and the system undergoes the ballistic expansion (BE). After the time of flight $T = 8.7$ ms a 2D absorption image of the cloud is taken in 50 μs with a horizontal beam [38]. Integration of 2D absorption images in the horizontal direction gives us the spatial distribution along the vertical z axis. Therefore we will consider only a 1D quantum-mechanical system along the vertical axis.

To confirm that a desired quantum state has been obtained (engineered) one can compare the spatial distributions along the vertical axis with the predicted ones. The coincidence of these spatial distributions is a necessary but not the sufficient requirement. A complete verification of the fidelity of the preparation of desired quantum states requires a quantum state reconstruction procedure. In order to perform this task we adopt the MaxEnt principle [30]. To do so we utilize a close analogy between quantum homodyne tomography [12] and the BE absorption imaging for the case of the point-like cloud (with the rms size equal to zero).

6.5.1 Motional States of Atoms via MaxEnt Principle: Formalism

In the quantum homodyne tomography the probability distributions are measured for the rotated quadrature operators $\hat{x}_\theta$. The annihilation and creation operators of motional quanta, $\hat{a}$ and $\hat{a}^\dagger$, are related to the position and momentum operators, $\hat{z}$ and $\hat{p}$, via expressions $\hat{z} = \frac{1}{\sqrt{2}}(\hat{a} + \hat{a}^\dagger)$ and $\hat{p} = \frac{1}{\sqrt{2}}i(\hat{a} - \hat{a}^\dagger)$, respectively. The angle θ of the quadrature operator corresponds to $\omega_z\tau$ and vertical "cuts" of the absorption images (taken after the BE) can be associated with quadrature probability distributions. However, for a real physical situation with a nonzero rms size of the cloud the vertical "cuts" of absorption images correspond to a coarse-grained quadrature probability distributions. In particular, the vertical cuts of measured absorption images (taken in 2D) give us (after integration along the horizontal direction) the spatial distribution along the vertical axis. The spatial distribution along

the vertical z axis can be expressed as (in order to reflect a different physical origin of the system under consideration in this section we will denote observables as $\hat{F}$ instead of $\hat{Q}$ that has been used in Sect. 6.4)

$$\overline{F}_\tau(z) = T^{-1} \int F_0(\xi_0) P_\tau((z-\xi_0)/T) d\xi_0 \,, \tag{6.69}$$

where $F_0(\xi_0)$ is the initial spatial distribution of the cloud in the z-direction (i.e., a Gaussian distribution with the rms size $\Delta\xi_0$). The function $P_\tau(v)$ denotes the velocity probability distribution of the measured quantum state which has been evolved for time τ in the harmonic potential before the BE, i.e.

$$P_\tau(v) = |\langle v|\psi(\tau)\rangle|^2, \qquad |\psi(\tau)\rangle = \hat{U}(\tau)|\psi(0)\rangle. \tag{6.70}$$

Here $\hat{U}(\tau) = \exp(-i\hat{H}\tau/\hbar)$ represents the time-evolution operator for the harmonic oscillator with the Hamiltonian $\hat{H} = \hat{p}^2/2m + m\omega_z^2\hat{z}^2/2$. Now we can treat the measured "cuts" as the mean values of specific observables: $\overline{F}_\tau(z) = \mathrm{Tr}\,[\hat{\rho}\hat{F}_\tau(z)]$. In practice just a few discrete times τ_j $(j = 1, \ldots, N_\tau)$ are considered and the z coordinate is discretized into the bins z_k $(k = -N_z, \ldots, N_z)$ of a given resolution Δz. The set of operators that enters the equation for the MaxEnt reconstruction then takes the form

$$\hat{F}_{\tau_j}(z_k) = T^{-1} \int F_0(\xi_0) \hat{U}^\dagger(\tau_j) \left| \frac{z_k - \xi_0}{T} \right\rangle \left\langle \frac{z_k - \xi_0}{T} \right| \hat{U}(\tau_j) d\xi_0 \,, \tag{6.71}$$

where $(j = 1, \ldots, N_\tau; k = -N_z, \ldots, N_z)$. We have already commented in Sect. 6.3 that the operator of mean phonon number $\hat{n}$ is added to the set of observables $\{\hat{F}_{\tau_j}(z_k)\}$. Knowledge of the mean excitation number $\bar{n}$ is essential in the case of an incomplete set of observables [30]. Knowledge of the mean excitation number leads to a natural "truncation" of the Hilbert space. The inclusion of the mean phonon number into the MaxEnt reconstruction scheme does not represent its limitation as the mean energy represents one of basic characteristics of any system that should be inferred from the measurement.

The experimental "cuts" of the BE absorption images $[\hat{F}_{\tau_j}(z)]$ can be taken at few selected times, for example $\omega_z\tau_j = 0, \pi/4, \pi/2, 3\pi/4$ $(N_\tau = 4)$. To perform the reconstruction we have to determine the Lagrange multipliers $\{\lambda_{j,k}\}$ and λ_n associated with $\{\hat{F}_{\tau_j}(z_k)\}$ and $\hat{n}$, respectively, in the expression for the generalized canonical density operator. The Lagrange multipliers can be determined via the minimization of a deviation function ΔF with respect to the measured data, i.e.

$$\begin{aligned} \Delta F = & \sum_{j,k} w_{j,k} \left\{ \overline{F}_{\tau_j}(z_k) - \mathrm{Tr}\left(\hat{\rho}_r \hat{F}_{\tau_j}(z_k) \right) \right\}^2 \\ & + w_{\bar{n}} \left\{ \bar{n} - \mathrm{Tr}\left(\hat{\rho}_r \hat{n} \right) \right\}^2 . \end{aligned} \tag{6.72}$$

Here $\{w_{j,k}\}$ and $w_{\bar{n}}$ represent positive weight factors for particular observables. Without any prior knowledge about the state, for simplicity we can take $w_{i,j} = 1$. The weight factor $w_{\bar{n}}$ associated with the mean phonon number can be chosen according to our preference either to fit better the "cuts" of the BE images or the mean phonon number. In the case of the perfect measurement and the complete reconstruction the result has to be independent of the choice of the weight factors (in this case we can take $w_{\bar{n}} = 1$). The weight factors could also be associated with the *prior* information about the dispersion of the measured observables. In particular, the weight factors can be taken as $w_\nu \sim \sigma_\nu^{-2}$ to reflect the knowledge of variances σ_ν for the measured observables $\hat{G}_\nu$. When the mean values of the observables for the MaxEnt estimate $\hat{\rho}_r$ fit within desired interval $\overline{G}_\nu \pm \sigma_\nu$ then contributions of the observables to the deviation function ΔF are of the same order (~ 1). However, in our case we do not assume the knowledge of variances for the measured discretized probability distributions (taking $w_\nu = 1$).

Once the Lagrange multipliers are numerically fitted, the result of the reconstruction – the generalized canonical density operator $\hat{\rho}_r$ – can be visualized, for example, via the corresponding Wigner function.

6.5.2 Numerical Simulation of MaxEnt Tomography

To test our reconstruction procedure let us consider the reconstruction of the Wigner function of the motional quantum state $|\psi(0)\rangle = (|0\rangle + |1\rangle)/\sqrt{2}$ of Cs atoms trapped in the optical lattice. This kind of state has been demonstrated in recent experiments [38]. We assume the following setup parameters: $\omega_z/2\pi = 80$ kHz, the rms size of the ground state $\Delta z_0 = 22$ nm, the rms velocity width $\Delta p_0/m = 11$ mm/s and the rms width of the cloud of the atoms about 60 μm. Before BE (with BE time $T = 8.7$ ms) the atoms evolve within the harmonic trapping potential for $\tau = 0, 1.6, 3.2, 4.8$ μs. As the input for the reconstruction via the MaxEnt principle four vertical "ideal" cuts of the BE absorption images are taken as shown in Fig. 6.6(b).

In addition, for the phonon number operator $\hat{n}$, which is included in the set of measured observables (see discussion above), we assume the mean value $\bar{n} = 0.5$. The result of the ideal reconstruction is shown in Fig. 6.6. The fidelity of the measured and the reconstructed quantum states is close to unity, which means a perfect reconstruction with $\Delta F = 10^{-10}$, entropy $S = 10^{-7}$, $\Delta\rho = 10^{-8}$ has been achieved. Here $\Delta\rho = \sum_{m,n} |(\hat{\rho} - \hat{\rho}_r)_{mn}|^2$ denotes a deviation of the original and reconstructed density operators.

Obviously, in a real measurement the measured values are always fluctuating around the exact ones due to an experimental noise. Therefore we simulate a non-ideal measurement introducing random fluctuations to the measured values of observables. It means that instead of the ideal values $\overline{F}_{\tau_j}(z_k)$ we use for the MaxEnt reconstruction procedure the fluctuating ("noisy") values

$$\overline{F}'_{\tau_j}(z_k) = \overline{F}_{\tau_j}(z_k) + \eta\xi_{j,k}\left(\overline{F}_{\tau_j}(z_k)\right)^{1/2}. \tag{6.73}$$

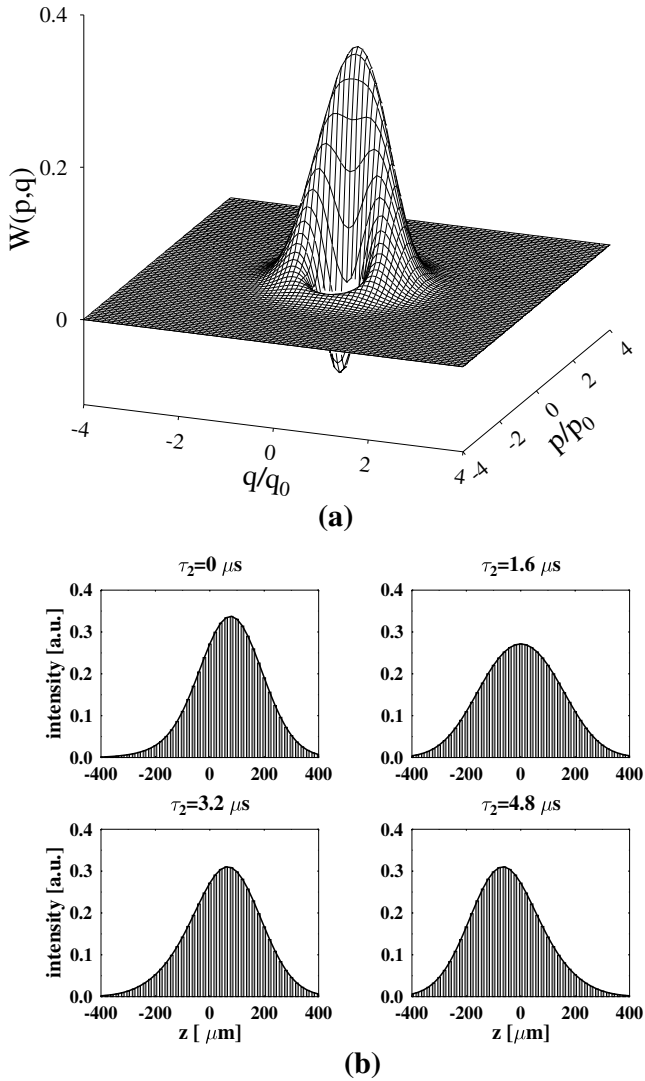

Fig. 6.6. (a) Numerical simulation of the reconstruction of the Wigner function of the motional quantum state $(|0\rangle + |1\rangle)/\sqrt{2}$ of Cs atoms trapped in the optical lattice (assuming $\omega_z/2\pi = 80$ kHz, the rms size of the ground state $\Delta z_0 = 22$ nm and the rms velocity width $\Delta p_0/m = 11$ mm/s). For the reconstruction via the MaxEnt principle four vertical cuts of the absorption images (with BE time $T = 8.7$ ms) have been taken (b). The histograms correspond to the measured data while the solid lines are obtained from the reconstructed Wigner function (i.e. they correspond to reconstructed marginal distributions). Before BE the atoms evolve within the trapping potential for the times $\tau = 0, 1.6, 3.2, 4.8$ μs. In addition, the mean number of motional quanta $\bar{n} = 0.5$ and the rms width of the cloud of the atoms about 60 μm have been assumed.

Here η is a relative-error parameter that characterizes the quality of the measurement and $\{\xi_{j,k}\}$ represents a Gaussian noise for observables. The result of the reconstruction is shown in Fig. 6.7 for $\eta = 0.1$. Noisy mean values of the observables are shown in Fig. 6.7(b). Inspite of a significant relative error, the reconstruction is almost perfect, with the fidelity of the measured and the reconstructed states still close to one ($\Delta F = 0.16$, entropy $S = 0.01$, $\Delta\rho = 0.05$). The minimum value of the deviation function $\Delta F = 0.16$ can serve also as a measure of the imperfection of the given measurement (due to a technical noise) [39].

A typical non-classical state that we can utilize for a further test is the even coherent state $\mathcal{N}_e(|\alpha\rangle + |-\alpha\rangle)$ [9]. We have presented a numerical simulation of the reconstruction of this state in Fig. 6.8. For the amplitude $\alpha = \sqrt{2}$ we obtained $\Delta F = 10^{-8}$, the entropy $S = 0.026$ and $\Delta\rho = 10^{-4}$ (under assumption that the exact mean phonon number $\bar{n} = 1.928$ is known). In the case of the imperfect measurement with $\eta = 0.1$ the reconstruction leads to $\Delta F = 0.14$, entropy $S = 0.13$, and $\Delta\rho = 0.06$ for $\bar{n} = 2.09$. The fidelity of the reconstructed and the measured states is, in this case, also close to one.

In order to model a technical noise in the measurement we have considered Gaussian fluctuations proportional to the square root of the mean values. It means that tails of the "cuts" of BE images do not introduce a significant error [compare Figs. 6.8(b) and 6.9(b)]. However, in the current measurements the situation seems to be different and the fluctuations do not decrease with the amplitude of the expected values.

The fundamental question in the context of the *MaxEnt* reconstruction of states from incomplete tomographic data is whether the quality of the reconstruction can be improved using additional data from subsequent time moments τ and how many such time moments τ are required for the complete reconstruction of the unknown state $\hat{\rho}$. As we have shown in Sect. 6.4 for the efficient quantum tomography just *three* quadrature distributions are sufficient for a complete reconstruction using the MaxEnt principle (in the case of the perfect measurement). This corresponds to the ideal case without the spatial dispersion of the cloud of atoms, i.e. the choice with $\omega_z\tau_j = 0, \pi/4, \pi/2$ ($N_\tau = 3$) is sufficient for $\Delta\xi_0 \to 0$. Obviously, in experiments with neutral atoms the spatial size of the atomic cloud is nonzero. However, in the case of the ideal measurement three BE absorption images associated with three "rotations" $\omega_z\tau_j$ are still sufficient for a complete reconstruction of tested examples of quantum states. On the other hand, it seems that for higher mean phonon numbers the spatial distributions along the vertical axis that are directly determined from absorption images should be known with improving precision (and on a wider interval of values as well). In the above examples we have considered for convenience BE images for four "rotations" ($N_\tau = 4$) which results in a very good reconstruction.

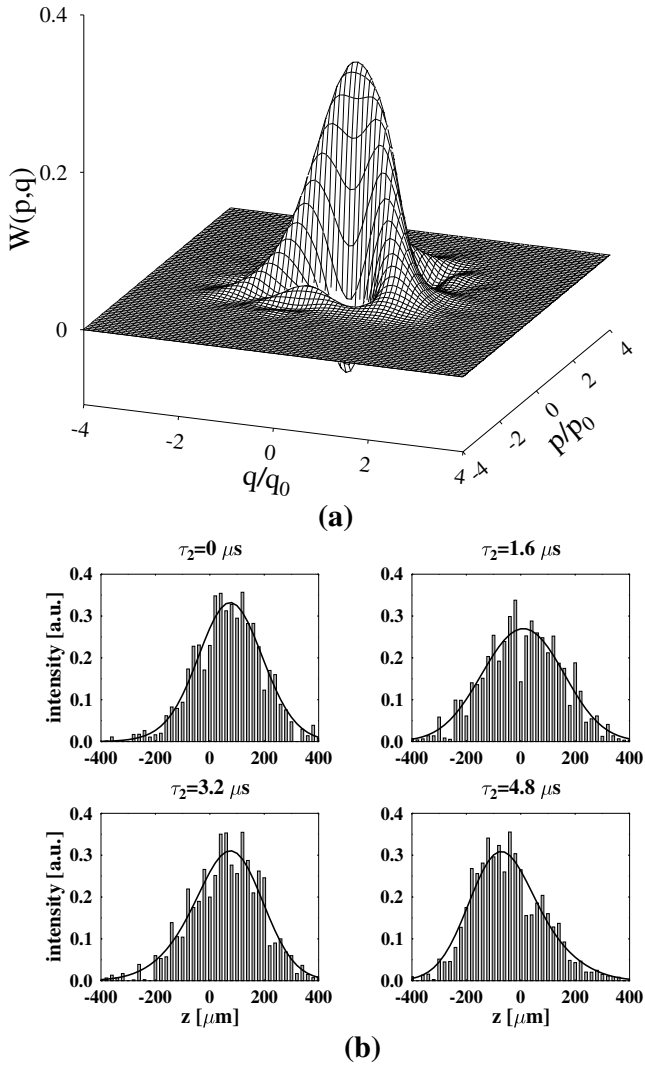

Fig. 6.7. (a) Numerical simulation of the reconstruction of the Wigner function of the atomic motional quantum state $(|0\rangle + |1\rangle)/\sqrt{2}$ for the same settings as in Fig. 6.6. (b) Four vertical cuts of the absorption images taken for reconstruction are fluctuating randomly around their ideal values shown in Fig. 6.6(b) with the relative error $\eta = 0.1$. The histograms correspond to the measured data while the solid lines are obtained from the reconstructed Wigner function. In addition, the mean phonon number $\bar{n}' = 0.6$ has been considered.

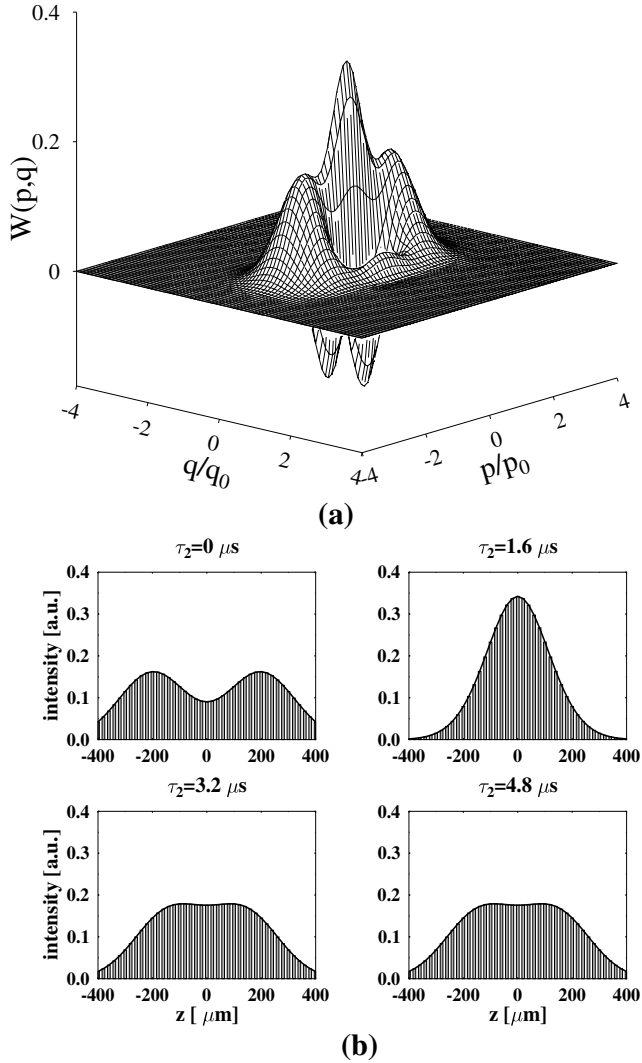

Fig. 6.8. Numerical simulation of the reconstruction of the Wigner function of the motional quantum state $\mathcal{N}_e(|\alpha\rangle + |-\alpha\rangle)$ with $\alpha = \sqrt{2}$ in the case of the ideal measurement. The mean number of motional quanta $\bar{n} = 1.928$. Other settings are the same as in Fig. 6.6.

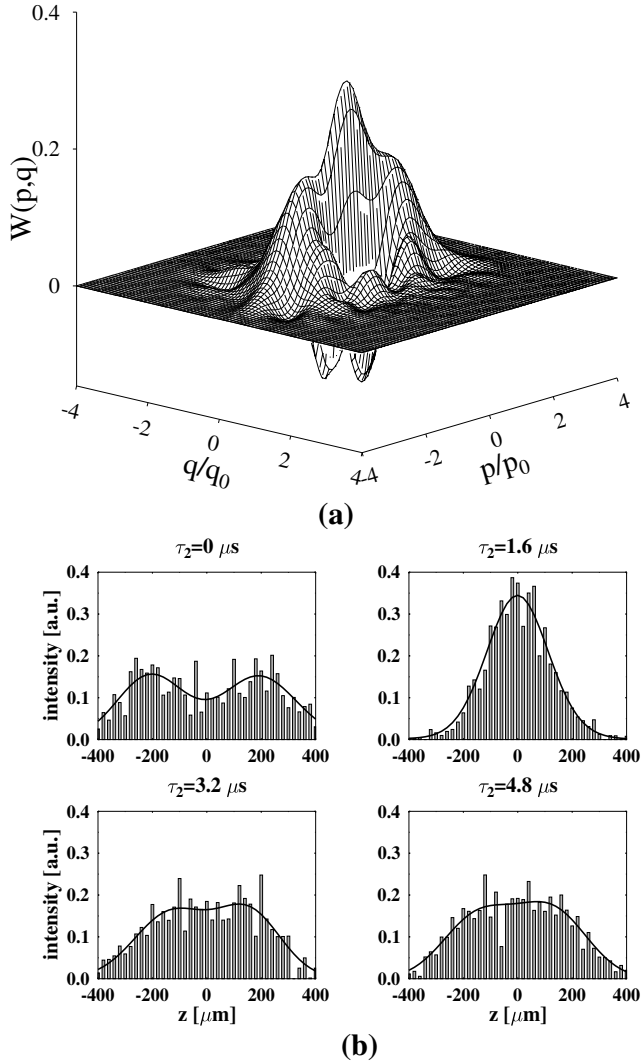

Fig. 6.9. Numerical simulation of the reconstruction of the Wigner function of the motional quantum state $\mathcal{N}_e(|\alpha\rangle + |-\alpha\rangle)$ with $\alpha = \sqrt{2}$ in the case of noisy measurement with $\eta = 0.1$. The "measured" mean number of the motional quanta $\bar{n}' = 2.09$. Other settings are the same as in Fig. 6.7.

6.5.3 Reconstruction from Experimental Data

In what follows we will apply the MaxEnt reconstruction scheme to the data obtained at the ENS in Paris [40]. Firstly we note that the unknown quantum state should belong to a Hilbert subspace that can be determined easily. Thus we can limit ourselves to the subspace spanned by Fock (number) states $|0\rangle, |1\rangle, \ldots |N-1\rangle$. The upper bound on the accessible phonon number N is given by experimental limitations such as, a feasible depth of microwells of the optical lattice and the validity of the harmonic potential approximation. For recent experiments N has been typically of the order of 10. This value is large enough to demonstrate the preparation of many non-classical states but on the other hand excludes highly squeezed states from coherent processing.

Let us consider the experimental arrangement used in Paris [40] with the parameters: $\omega_z/2\pi = 80$ kHz, the rms size of the ground state $\Delta z_0 = 22$ nm, the rms velocity width $\Delta p_0/m = 11$ mm/s, the rms width of the cloud of the atoms about 60 μm and BE time $T = 8.7$ ms. Initially the atoms are prepared in a well-defined motional state $|\psi_0\rangle$ (e.g. in the vacuum state $|0\rangle$). Then the optical lattice is switched off for the time period t_1 during which the atoms evolve freely towards the state $|\psi_1\rangle = \exp(-it_1\hat{p}^2/2m)|\psi_0\rangle$. Next, the optical lattice is again switched on for the time τ during which the atoms evolve within the harmonic trapping potential. The measurement is performed after the BE time. The first two stages can be considered as the preparation of the state $|\psi_1\rangle$. After its "rotation" by $\omega_z\tau$ (within the phase space of the harmonic oscillator) and the subsequent BE the absorption images are taken.

The considered data are for the initial vacuum state which means that under ideal conditions a squeezed state $|\psi_1\rangle = \exp(-it_1\hat{p}^2/2m)|0\rangle$ should be prepared. The vertical spatial distributions obtained from the measured 2D-absorption images are discretized into pixels (bins) with the pixel width 5.45 μm. The optical density of each pixel is averaged in the horizontal direction in which the absorption images are divided into 50 rows, each 3.9 μm wide (these rows cover the size of the cloud in the horizontal direction). For the reconstruction via the MaxEnt principle four vertical spatial distributions for "rotation" times $\tau = 0, 1.6, 3.2$ and 4.8 μs are taken. The selected times roughly correspond to rotations within the phase space by $\omega_z\tau = 0, \pi/4, \pi/2$ and $3\pi/4$, respectively. Unfortunately, the mean excitation number $\hat{n}$ for measured state $|\psi_1\rangle$ was not measured explicitly in the experiment, therefore we have to estimate it as follows: During the free expansion period the rms size of the cloud increases by $\Delta x = p_0\tau_1/m$. The corresponding increase of the potential energy $\frac{1}{2}m\omega_z^2(\Delta x)^2$ in units $\hbar\omega_z$ gives us the increase of the number of excitation quanta with respect to the initial state $|\psi_0\rangle$. For $\tau_1 = 4$ μ and the initial vacuum it means $\bar{n} \approx 1$. Experiments can be realized also for higher τ_1. For example, $\tau_1 = 8$ μ leads to $\bar{n} \approx 4$. However, as mentioned above, such "squeezed" states with a significant contribution of higher phonon number states violate the underlying harmonic approximation for the potential. To

keep a coherent control an anharmonic part of the potential has to be taken into account.

The result of the reconstruction via the MaxEnt principle is shown in Fig. 6.10. The deviation of the fitted and measured values is $\Delta F = 0.09$ and the entropy of the reconstructed state is $S = 1.0$. It means that the reconstructed state is a statistical mixture. We see a two peak structure that suggests that there is a mixture of two squeezed states coherently displaced from each other. It is caused by the fact that the vertical center of the cloud was not fixed in the experiment and it has to be determined by our fit for each measured BE absorption image separately. Assuming a priori knowledge that the Wigner function has a symmetric shape with respect to the origin of the phase space (i.e. there is no coherent amplitude) a Gaussian fit can be used to determine the center of the cloud for each vertical distribution. For states with a non-zero coherent amplitude the center of the cloud should be fixed already in the experiment.

It turns out that the reconstruction results do not describe the squeezed vacuum state as was originally expected [40]. The main reason is that the mean phonon number was not measured directly in the experiment. It can be inferred only indirectly from the ideal case without any incoherence during preparation or measurement. As we discussed above, it is essential to include the information about the mean number of vibrational quanta into the MaxEnt reconstruction scheme. In optical tomography the analogous information about mean photon number can be obtained from distributions of two "orthogonal" quadratures. In our case it could correspond to two absorption images such that $\omega_z(\tau_j - \tau_k) = \pi/2$. However, it would require a precise timing of the evolution within the harmonic trapping potential. Therefore the mean number of vibrational quanta should be determined in an independent measurement.

Another problem arises from a slow convergence of anti-squeezed spatial distributions that are derived directly from the measured absorption images. In particular, the convergence of tails is too slow for those "rotations" that correspond to anti-squeezed phases, i.e. $\tau = 1.6, 4.8\ \mu$s [see Fig. 6.10(b)]. The slow convergence is reflected by the presence of non-negligible backgrounds for Gaussian fits to these spatial distributions. If we eliminate (subtract) these backgrounds from the measured distributions the MaxEnt reconstruction gives almost the same Wigner function as in Fig. 6.10(a) but with a highly reduced deviation function $\Delta F = 0.02$ (comparing to $\Delta F = 0.09$ in Fig. 6.10). Such background in these absorption images can be caused by an incoherence associated with a violation of the the harmonic approximation. In fact, in our analysis we have neglected the change of the oscillation frequency along the z-axis. In recent experiments, the oscillation frequency decreases 10% from ω_z for microwells at the edge of the initial cloud.

In this section we have applied the *MaxEnt* scheme for a reconstruction of motional quantum states of neutral atoms. As an example we have analyzed the experimental data obtained by the group of C. Salomon at the ENS in

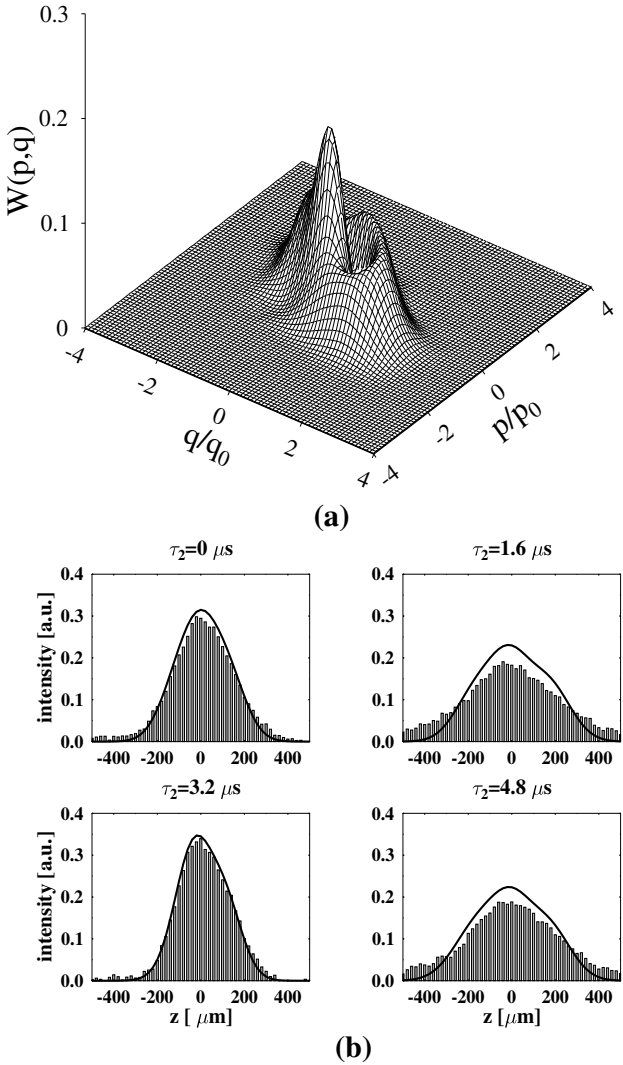

Fig. 6.10. The Wigner function reconstructed from the experimental data obtained at the ENS, Paris. The experimental setting is the same as for Fig. 6.6. From the experimental data we have inferred the mean number of motional quanta $\bar{n} \approx 1.0$, while the reconstructed value is $\bar{n}' \approx 1.1$. Deviation of the measured and predicted values of observables is $\Delta F = 0.09$ and entropy of the reconstructed mixture state is $S = 1.0$. Subtraction of a background from the measured marginals gives almost the same Wigner function and reduces significantly a difference between measured and reconstructed marginals.

Paris and we reconstruct the Wigner function of motional quantum states of Cs atoms trapped in the optical lattice. In our analysis we have neglected the change of the oscillation frequency along z axis in recent experiments. The dispersion of the oscillation frequency is of the order of a few percent. This source of errors can significantly affect the quality of a quantum state preparation and its reconstruction. In addition, only up to the first 10 bound states of microwells of the optical lattice can be approximated by a harmonic potential. It implies limits on coherent manipulations of quantum states. It means that states with a significant contribution of higher number (Fock) states cannot be prepared and manipulated in a controlled way.

6.6 Direct Measurement of Wigner Functions of Single Mode Fields in Cavities

We have shown in previous sections that Wigner functions of bosonic fields can be reconstructed from the tomographic data either via the inverse Radon transformation or using the method of pattern functions. In the case where the experimental data are not complete both these procedures can be substituted by a very efficient method of reconstruction based on the MaxEnt principle. Recently several groups have discussed the possibility of performing a reconstruction of Wigner functions of bosonic fields based on other tomographic measurements. Specifically, Englert *et al.* [41] have shown that the Wigner function can be measured *directly* via a measurement of the parity operator of the bosonic field. This method has been further developed by Lutterbach and Davidovich [42]. The essence of the method is based on a simple relation between the value of the Wigner function $W(\alpha)$ at a phase-space point α and the mean value of the parity operator $\hat{P}$:

$$W(\alpha) = 2\mathrm{Tr}\left[\hat{D}(-\alpha)\hat{\rho}\hat{D}(\alpha)\hat{P}\right] , \tag{6.74}$$

where the $\hat{D}(\alpha) = \exp(\alpha\hat{a}^\dagger - \alpha^*\hat{a})$ is displacement operator [see also (6.8)] and the field parity operator $\hat{P}$ is defined as

$$\hat{P} = \exp\left[i\pi\ \hat{a}^\dagger\hat{a}\right] . \tag{6.75}$$

This operator acts on a Fock state $|n\rangle$ as $\hat{P}|n\rangle = (-1)^n|n\rangle$. With this normalization, $-2 \leq W \leq 2$ and $\int W(\alpha)\ d^\alpha = \pi$ (see also Sect. 6.2.2).

Lutterbach and Davidovich have shown that if the single-mode field in the state $\hat{\rho}$ is stored in a cavity C and if it can be shifted (displaced) by injecting in C a coherent field with an amplitude $-\alpha$, then one can perform a measurement of the parity operator $\hat{P}$ on the resulting field $\hat{\rho}(\alpha) = \hat{D}(-\alpha)\hat{\rho}\hat{D}(\alpha)$. Repeating this measurement many times for each value of α, one obtains a

value of the Wigner function at the given phase-space point α

$$\frac{W(\alpha)}{2} = \mathrm{Tr}\left[\hat{\rho}(\alpha)\,\hat{P}\right] = \langle \hat{P} \rangle = \sum_{n=0}^{\infty} (-1)^n \rho_{nn}(\alpha)\ . \tag{6.76}$$

In order to measure the mean value of the parity operator $\langle \hat{P} \rangle$ in the cavity it is enough to send across the cavity a sequence of two-level atoms with a known velocity. The transition between two levels (denoted as $|e\rangle$ and $|g\rangle$, respectively) of each atom is slightly de-tuned from the resonance with the cavity mode (the frequency mismatch is denoted as Δ). When the cavity mode is in a Fock state $|n\rangle$ the atomic transition frequency is light shifted at the center of the cavity by $\Omega^2 n/2\Delta$ where Ω is the resonant vacuum Rabi frequency (see for instance [43]). The frequency mismatch Δ is chosen so that a single-photon process produces a π-phase shift on an $|e\rangle \to |g\rangle$ transition during the atom-cavity interaction time (that is dictated by the velocity of the atom).

As shown by Lutterbach and Davidovich this phase shift can be determined (measured) by the Ramsey interferometry [44] by subjecting each atom to two resonant $\pi/2$ pulses that mix $|e\rangle$ and $|g\rangle$ levels of the atom before and after the interaction with the cavity field. The probability p_e (p_g) to detect the atom at the exit from the cavity in the state $|e\rangle$ ($|g\rangle$) exhibits modulations with respect to the phase ϕ of the interferometer. For a cavity that has been prepared in the vacuum state $|0\rangle$ and a proper choice of the phase reference the probability p_e oscillates as $p_e(\phi) = (1+\cos\phi)/2$. The phase shift induced by the n-photon field is $n\phi$. Correspondingly, the probability to find an atom in the exited state $|e\rangle$ when the cavity mode is displaced by α reads

$$\begin{aligned} p_e(\phi,\alpha) &= \left[1 + \sum_{n=0}^{\infty} (-1)^n \rho_{n,n}(\alpha)\cos\phi\right]/2 \\ &= \left[1 + \langle \hat{P} \rangle \cos\phi\right]/2\ . \end{aligned} \tag{6.77}$$

From above we see that the Wigner function at the phase-space point α is directly related to the fringes contrast $c(\alpha)$:

$$\begin{aligned} W(\alpha) &= 2\langle \hat{P} \rangle = 2c(\alpha) \\ &= 2\left[p_e(0,\alpha) - p_e(\pi,\alpha)\right]\ . \end{aligned} \tag{6.78}$$

In other words the Wigner function of the cavity field is determined from the expectation values of a measurement performed on the atom after its interaction with the displaced cavity mode. The attractive feature of this procedure is that there is no need to perform any further inversion procedure to determine the value of the Wigner function at the given phase-space point. On the other hand, to determine the complete Wigner function one has to "scan" the whole phase space, i.e. one has to displace the original cavity mode with a continuum set of values of α.

The group of Serge Haroche from the ENS in Paris has recently reported [45] experimental realization of the Lutherbach-Davidovich method. The experiment itself has been very challenging since a large dispersive phase shift per photon had to be achieved. In addition the measurement itself has to be performed in a time that is shorter than the field damping time. Technical details of the experiment and the description of the cavity QED setup can be found in [45] and [46], respectively. In what follows we will utilize the data obtained in the experiment. In particular, Haroche *et al.* have performed the direct measurement of the Wigner function for the vacuum state and the one-photon Fock state. In their experiment only a finite set of the values $W(\alpha)$ of the Wigner function for *real non-negative* α have been measured. In Fig. 6.11 data from the measurement of the Wigner function of a vacuum cavity field are presented. Analogously, in Fig. 6.12 data from the measurement of the Wigner function of a single-photon Fock state of the cavity field are shown.

Given the experimental data and *a priori* knowledge that the cavity mode is initially prepared in a phase-insensitive state, one might conclude that the experimental data presented in Figs. 6.11 and 6.12 correspond to the vacuum state and the one-photon Fock state of the cavity field. Nevertheless, a conservative approach is more appropriate, that is the reconstruction of the Wigner function has to be warranted only by experimental data (i.e., the mean values of the parity operator for given values of α) and no further assumptions should be made. Under this circumstance, we can utilize the reconstruction scheme based on the principle of Maximum Entropy as described in previous sections of this chapter. Here the observables are the displaced parity operators $\hat{D}(\alpha)\hat{P}\hat{D}^{\dagger}(\alpha)$ for various discrete values of real non-negative parameter α. In order to use the MaxEnt reconstruction scheme as discussed in Sect. 6.3 we also have to know the mean-value of the photon number operator of the cavity field. Unfortunately, this operator has not been measured in the experiment, so this number is only estimated from the experimental data. With these inputs we can perform the reconstruction of Wigner function.

In Fig. 6.13 we present a reconstruction of the Wigner function of the cavity mode based on the experimental data presented in Fig. 6.11.

The reconstructed Wigner function is asymmetric since the data obtained from the measurement do not warrant any phase symmetry. The mean-photon number is not a direct observable, it is not a constraint in the MaxEnt reconstruction scheme. From the reconstructed Wigner function one obtains the mean-photon number $\bar{n} \simeq 0.3$ and the photon number distribution $P_n \simeq \{0.88, 0.07, 0.00, \dots\}$.

In principle one can assume that the measured data are rotationally invariant. That is, if in the direction of other rotated quadrature the same mean values of the displaced parity operator are measured, then utilizing this additional (though not warranted by the measured data) information we can use the MaxEnt principle again and perform the reconstruction with these additional mean-values of the "measured" parity operators. In Fig. 6.14 we present the reconstruction of the Wigner function under the assumption that

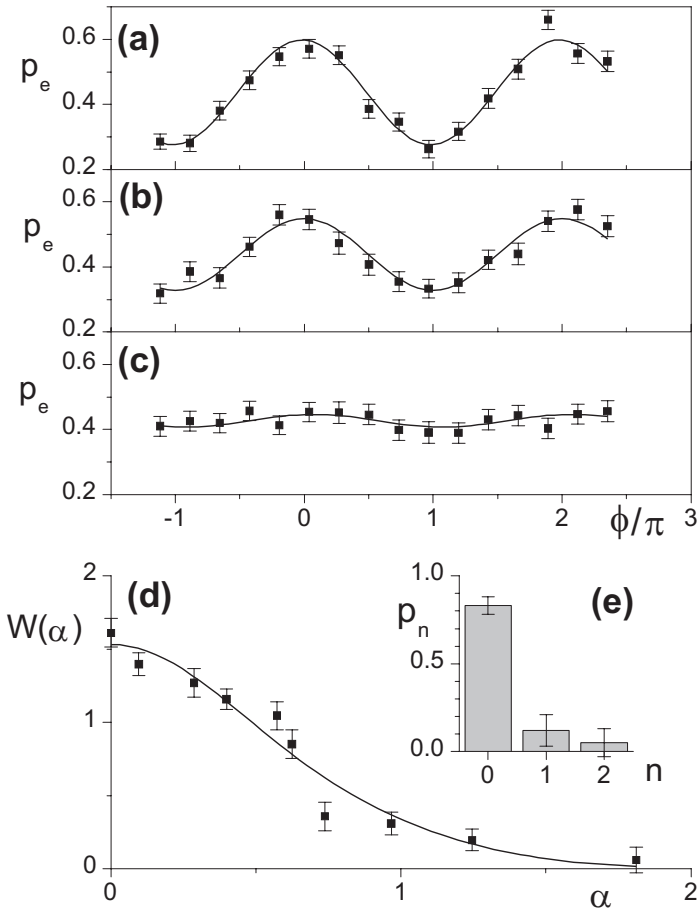

Fig. 6.11. Results of the measurement of a set of values $W(\alpha)$ of the Wigner function of a single-mode cavity field. (a) Ramsey fringes for an injected amplitude $\alpha = 0$. Probability p_e for detecting the atom in the state $|e\rangle$ as a function of the Ramsey interferometer phase ϕ/π. Dots are experimental with error bars reflecting the variance of the binomial detection statistics. The solid curve is a sine fit. (b) and (c) Ramsey fringes for $\alpha = 0.57$ and $\alpha = 1.25$, respectively. (d) Dots represent experimentally measured values of the Wigner function versus the phase-space parameter α with error bars reflecting the uncertainty in the Ramsey fringes fit. The solid line represents a theoretical fit performed by Haroche *et al.*. (e) Corresponding photon number distribution. The figure is shown with the kind permission of J.M. Raimond.

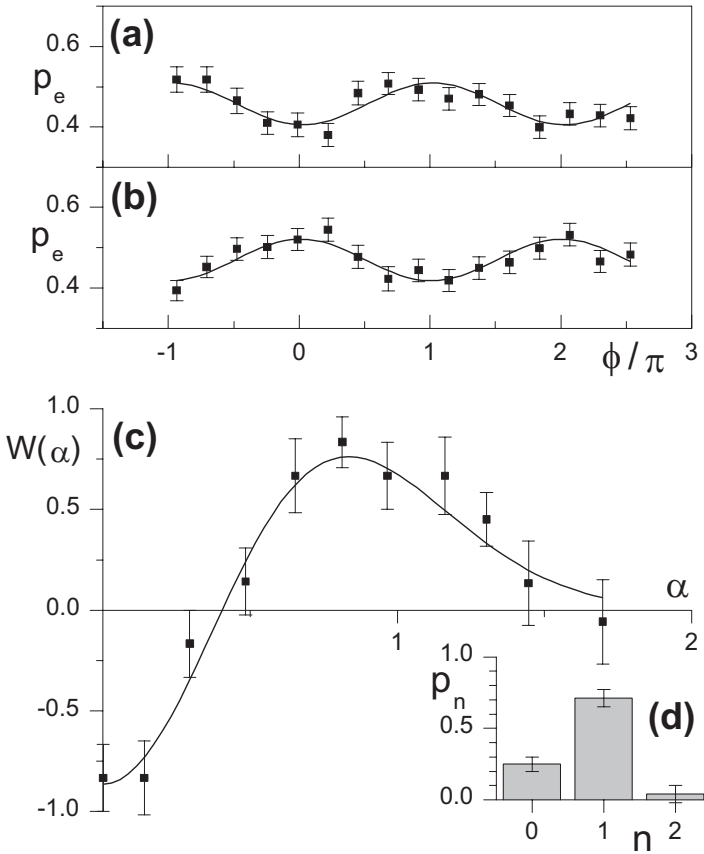

Fig. 6.12. Results of the measurement of a set of values $W(\alpha)$ of the Wigner function of a single-mode cavity field. Here a single-photon field has been initially prepared in the cavity. (a) Ramsey fringes for an injected amplitude $\alpha = 0$. Probability p_e for detecting the atom in the state $|e\rangle$ as a function of the Ramsey interferometer phase ϕ/π. Dots are experimental with error bars reflecting the variance of the binomial detection statistics. The solid curve is a sine fit. (b) Ramsey fringes for $\alpha = 0.81$. (c) Dots do represent experimentally measured set of values of the Wigner function versus the phase-space parameter α with error bars reflecting the uncertainty on the Ramsey fringes fit. The solid line represents a theoretical fit performed by Haroche *et al.*. (d) Inferred photon number distribution. The figure is shown with the kind permission of J.M. Raimond.

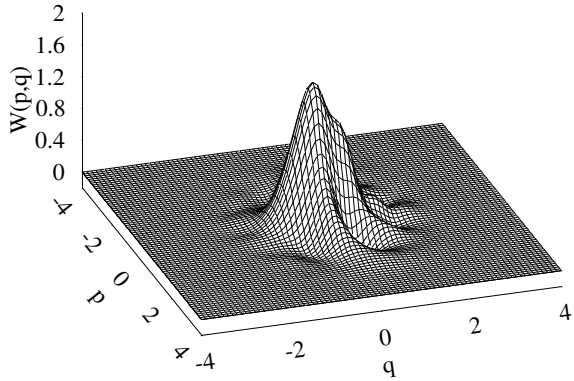

Fig. 6.13. The Wigner function for the vacuum-like state (with the mean photon number $\bar{n} = 0.22$ determined from the measured data) reconstructed via the MaxEnt principle. The measured observable - the shifted parity operator - corresponds to the direct measurement of the Wigner function $W(x_j, 0)$ at $\{x_j, j = 1, ..., 10\}$. Here I denote $x_j = \alpha$.

the same set of values of the Wigner functions has been measured for 16 values of angles of rotation. It is interesting to note, that from the reconstructed Wigner function one obtains the mean-photon number $\bar{n} \simeq 0.285$ and the photon number distribution is equal to $P_n \simeq \{0.835, 0.084, 0.042, 0.039 \dots\}$. That is, from the MaxEnt reconstruction scheme under the given assumptions we obtain a non-zero probability of occupation of the Fock state $|3\rangle$ that has not been considered by the authors of the experiment (see [45]). In the figure we also plot the distribution $W(x, 0)$ that is obtained from the MaxEnt reconstruction scheme and we compare it with the experimental data (displayed as $\star$). We see that the MaxEnt scheme very nicely reconstructs the Wigner function of the cavity mode. This state is not exactly the vacuum, but rather a thermal mixture at a very low temperature.

Let us consider the reconstruction of the Wigner function based on the experimental data presented in Fig. 6.12.

This reconstructed Wigner function is asymmetric (see Fig. 6.15) since the data obtained from the measurement do not warrant any phase symmetry. The mean-photon number is not a direct observable, it is not a constraint in the MaxEnt reconstruction scheme. From the reconstructed Wigner function one obtains the mean-photon number $\bar{n} \simeq 0.82$ and the photon number distribution $P_n \simeq \{0.28, 0.70, 0.00, \dots\}$.

We can again make an assumption about the fact that the displaced parity operator is measured for different values of the phase-space rotations (i.e. down different rotated quadratures). In this case we can extend the observation level and perform a new reconstruction via the MaxEnt principle. In Fig. 6.16 we assume that the displaced parity operator has been measured for 20 values of phases. That is, we consider 20 rotations of the original dis-

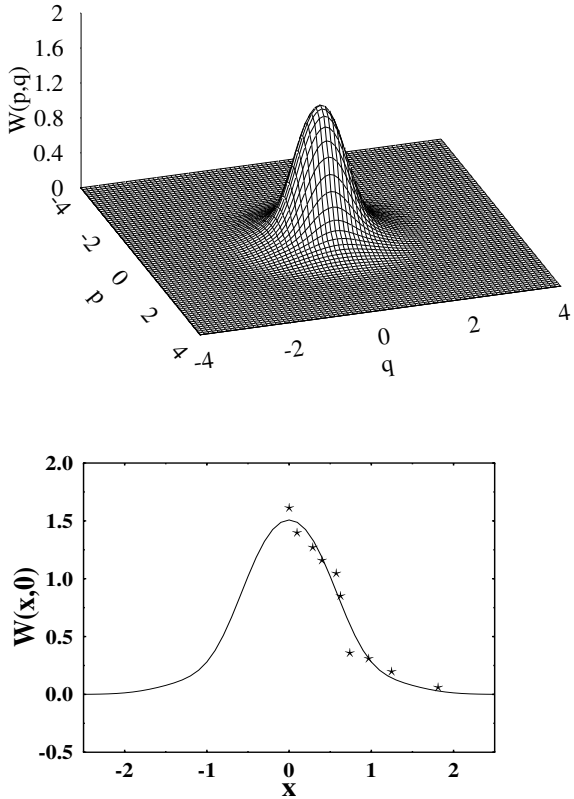

Fig. 6.14. The Wigner function for the vacuum-like state (with the "measured" mean value of the photon number $\bar{n} = 0.22$) reconstructed via the MaxEnt principle. The measured observable - the shifted parity operator - corresponds to the direct measurement of the Wigner function $W(x_j, 0)$ at $\{x_j, j = 1, ..., 10\}$. We consider the same setting as in Fig. 6.13 but we perform a reconstruction under the assumption that the distribution $W(x_j, \phi_n)$ has been measured for 16 values of the angles, i.e. $\phi_n = n\pi/8$. In the figure we also plot the distribution $W(x, 0)$ that is obtained from the MaxEnt reconstruction scheme and we compare it with the experimental data (displayed as $\star$).

tribution $W(x_j, 0)$. For pedagogical purposes we will consider two situations: first we consider these 20 angles to be chosen randomly. In the second case the angles are regular, with $\phi_n = n\pi/10$.

Intuitively it is clear that once we extend the observation level, i.e. we increase the number of angles for which the displaced parity operator is measured, we should obtain a better reconstruction. This is nicely illustrated in the lower picture in Fig. 6.16 that really reminds the Wigner function of the single-photon Fock state. The difference between the upper and lower figures is only in the distribution of phases. In the upper case phases are random

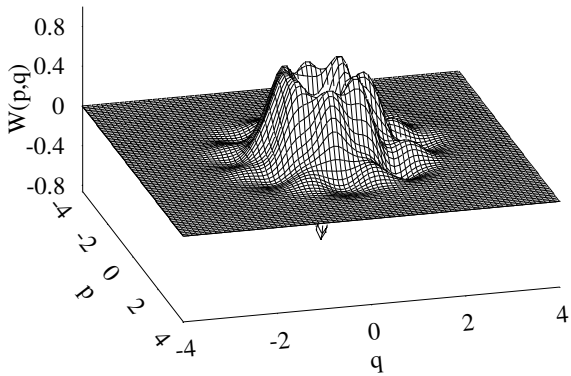

Fig. 6.15. The Wigner function for the single-photon-like state (with the "measured" meanvalue of the photon number $\bar{n} = 0.79$) reconstructed via MaxEnt principle. The measured observable - the shifted parity operator - corresponds to the direct measurement of the Wigner function $W(x_j, 0)$ at $\{x_j, j = 1, ..., 10\}$.

in the lower case phases are regular. So the question is why there is such a difference between the two figures that has been obtained from the same experimental data and using the same reconstruction scheme. The reason is purely numerical. In the case of random phases the dimension of the Hilbert space that is used for the MaxEnt reconstruction has to be larger. The oscillations of the reconstructed Wigner function in the top figure have their origin in a wrong assumption about the dimension of the Hilbert space that has to be considered in the reconstruction (see discussion in Sect. 6.4). This example illustrates that one has to be very careful with handling the data.

Finally, in Fig. 6.17 we present a comparison between the reconstructed distribution $W(x, 0)$ and measured values of $W(x_j, 0)$ obtained in the measurement.

6.7 Conclusions

We have shown that the reconstruction of Wigner functions from incomplete tomographic data can be very reliably performed with the help of the Jaynes principle of the Maximum Entropy. He have presented a generalized canonical density operator that is suitable for the incomplete tomographic data. We have implemented a numerical procedure with the help of which the *MaxEnt* reconstruction can be performed. We have compared the *MaxEnt* scheme with the sampling via pattern functions. The comparison is very clear - the *MaxEnt* approach is much more efficient. It requires less data, it gives the reconstruction with much higher fidelity and is more stable with respect to the choice of parameters such as the size of the quadrature bin, or the interval on which the quadrature distributions are measured. Our empirical experience

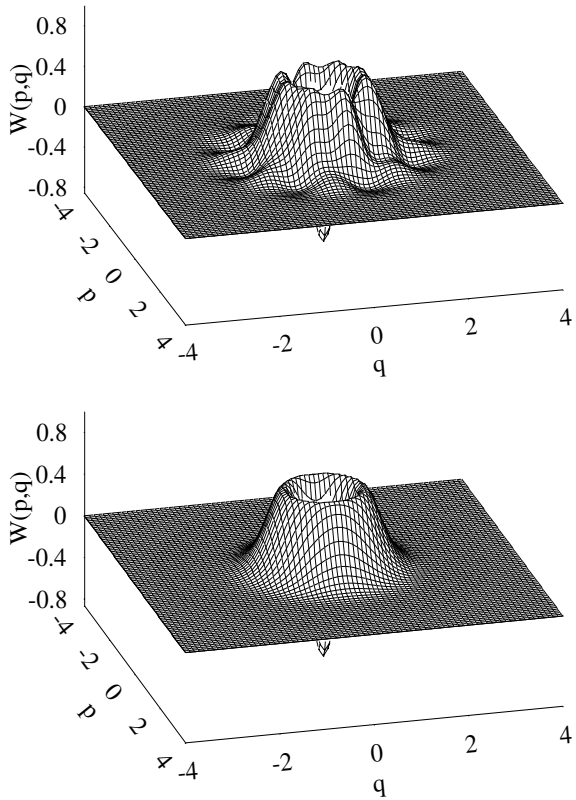

Fig. 6.16. The Wigner function for the one-photon Fock state (with the "measured" mean value of the photon number $\bar{n} = 0.79$) reconstructed via the MaxEnt principle. The measured observable - the shifted parity operator - corresponds to the direct measurement of the Wigner function $W(x_j, 0)$ at $\{x_j, j = 1, ..., 10\}$. The reconstruction of the Wigner function is performed under the assumption that the distribution $W(x_j, \phi_n)$ has been measured for 20 values of the phase, while $W(x_j, \phi_m) = W(x_j, \phi_n)$. The upper figure corresponds to the situation when the angles have been chosen randomly, the bottom figure corresponds to the regular case when $\phi_n = n\pi/10$.

shows that three rotated quadratures are always sufficient to perform a very reliable *MaxEnt* reconstruction of an arbitrary unknown state.

In this chapter the method has been demonstrated on two sets of experimental data. Firstly, we have reconstructed vibrational states of neutral atoms. Secondly, we have performed a reconstruction of a single-mode electromagnetic field inside a high-Q cavity. In both these examples the efficiency of the proposed method is clearly seen. Recently, our method based on the Jayne's principe of maximum entropy has been applied (see [47]) for the tomographic reconstruction of a complete internuclear quantum state, represented

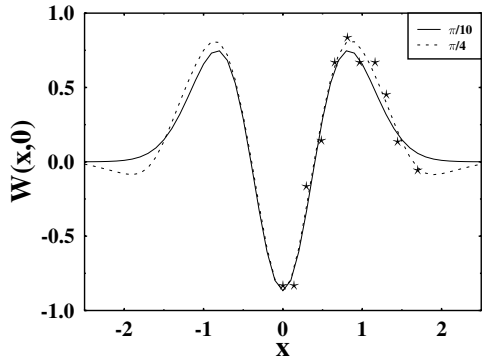

Fig. 6.17. The distribution $W(x,0)$ that is obtained from the MaxEnt reconstruction scheme of the Fock state $|1\rangle$ under two assumptions. The number of angles for which the distribution $W(x_j,\phi_n)$ is 8 (dotted line) and 20 (solid line). We compare these distributions with the experimental data (displayed as $\star$).

by the Wigner function, of a dissociating I_2 molecule based on femtosecond time resolved position and momentum distributions of the atomic fragments. These examples illustrates versatility of the MaxEnt reconstruction scheme and its efficiency it situations when mean values of a restricted set of observables have been measured.

Acknowledgements

I would like to thank Gabriel Drobný for a longstanding collaboration and numerous discussions devoted to technical as well as conceptual problems related to reconstruction of states of quantum systems. I also thank Christophe Salomon and Isabelle Bouchoule (experiment with neutral atoms) and Michel Brune and Jean-Michel Raimond (cavity QED experiment) for providing me with their experimental data and for helpful discussions and correspondence. This work was supported by the European Union projects QGATES and (CON)QUEST.

References

1. E.T. Jaynes: Information theory and statistical mechanics. In: *1962 Brandeis Lectures*, vol 3, ed by K.W. Ford (Benjamin, Elmsord, New York 1963) p 181
2. A. Peres: *Quantum Theory: Concepts and Methods* (Kluwer Academic Publishers, Dordrecht, 1995)
3. R. Omnès: *The Interpretation of Quantum Mechanics* (Princeton University Press, Princeton, NJ, 1994)
4. L.E. Ballentine: *Quantum Mechanics* (Prentice Hall, Englewood Cliffs, New Jersey, 1990)

5. Z. Hradil, J. Řeháček, J. Fiurášek, M. Ježek, Maximum-Likelihood Methods in Quantum Mechanics, Lect. Notes Phys. **649**, 59–112 (2004)
6. V. Bužek and R. Derka: *Quantum observations.* In *Coherence and Statistics of Photons and Atoms*, ed by J. Peřina (John Wiley & Sons, New York, 2001) pp 198 - 261
7. E.P.Wigner: Phys. Rev. **40**, 749 (1932)
8. M. Hillery, R.F. O'Connell, M.O. Scully, and E.P. Wigner: Phys. Rep. **106**, 121 (1984)
9. V. Bužek and P.L. Knight: Quantum interference, superposition states of light and nonclassical effects. In *Progress in Optics*, vol 34, ed by E. Wolf (North Holland, Amsterdam, 1995) p.1
10. A.K. Ekert and P.L. Knight: Phys. Rev. A **43**, 3934 (1991)
11. K. Vogel and H. Risken: Phys. Rev. A **40**, 2847 (1989)
12. U. Leonhardt: *Measuring the quantum state of light.* (Cambridge University Press, Cambridge, 1997)
13. D.-G. Welsch, W.Vogel, and T. Opatrný: Homodyne detection and quantum state reconstruction. In *Progress in Optics*, vol 39, ed by E. Wolf (North Holland, Amsterdam, 1999) p.63
14. G.M. D'Ariano, C. Machiavelo, and M.G.A. Paris: Phys. Rev. A **50**, 4298 (1994)
15. H. Kühn, D.-G. Welsch, and W. Vogel: J. Mod. Opt. **41**, 1607 (1994)
16. D.T. Smithey, M. Beck, M.G. Raymer, and A. Faridani: Phys. Rev. Lett. **70**, 1244 (1993);
    D.T. Smithey, M. Beck, J. Cooper, and M.G. Raymer: Phys. Scr. T **48**, 35 (1993);
    M. Beck, M.G. Raymer, I.A. Walmsley, and V. Wong: Opt. Lett. **18**, 2041 (1993).
    M. Beck, D.T. Smithey, and M.G. Raymer: Phys. Rev. A **48**, R890 (1993);
    M.G. Raymer, M. Beck, and D.F. Mc Alister: Phys. Rev. Lett. **72**, 1137 (1994);
    M.G. Raymer, D.T. Smithey, M. Beck, and J. Cooper: Acta Phys. Pol. **86**, 71 (1994)
17. M. Munroe, D. Boggavarapu, M.E. Anderson, and M.G. Raymer: Phys. Rev. A **52**, R924 (1995)
18. U. Janicke and M. Wilkens: J. Mod. Opt. **42**, 2183 (1995)
19. S. Schiller, G. Breitenbach, S.F. Pereira, T. Müller, and J. Mlynek: Phys. Rev. Lett. **77**, 2933 (1996);
    Ch. Kurtsiefer, T. Pfau, and J. Mlynek: Nature **386**, 150 (1997).
20. S. Wallentowitz and W. Vogel: Phys. Rev. Lett. **75**, 2932 (1995);
    J.F. Poyatos, R. Walser, J.I. Cirac, P. Zoller, and R. Blatt: Phys. Rev. A **53**, R1966 (1996);
    C.D'Helon and G.J. Milburn: Phys. Rev. A **53**, R25 (1996)
21. D. Leibfried, D.M. Meekhof, B.E. King, C. Monroe, W.M. Itano, and D.J. Wineland: Phys. Rev. Lett. **77**, 4281 (1996);
    D. Leibfried, D.M. Meekhof, C. Monroe, B.E. King, W.M. Itano, and D.J. Wineland: J. Mod. Opt. **44**, 2485 (1997);
    D. Wineland, C. Monroe, D.M. Meekhof, B.E. King, D. Liebfried, W.M. Itano, J.C. Bergquist, D. Berkeland, J.J. Bollinger, and J.Miller: Proc. Roy. Soc. A **454**, 411 (1998)
22. T.J. Dunn, I.A. Walmsley, and S. Mukamel: Phys. Rev. Lett. **74**, 884 (1995)
23. U. Leonhardt, H. Paul, and G.M. D'Ariano: Phys. Rev. A **52**, 4899 (1995)

24. Th. Richter: Phys. Lett. A **211**, 327 (1996);
Th. Richter: Phys. Rev. A **53**, 1197 (1996)
25. U. Leonhardt, M. Munroe, T. Kiss, T. Richter, and M.G. Raymer: Opt. Commun. **127**, 144 (1996)
26. G.M. D'Ariano, U. Leonhardt, and H. Paul: Phys. Rev. A **52**, R1801 (1995)
27. J. von Neumann: *Mathematical Foundations of Quantum Mechanics* (Princeton University Press, Princeton, 1955)
28. A. Wehrl: Rev. Mod. Phys. **50**, 221 (1978)
29. E. Fick and G. Sauermann: *The Quantum Statistics of Dynamic Processes.* (Springer Verlag, Berlin, 1990)
30. V. Bužek, G. Adam, and G. Drobný: Ann. Phys. (N.Y.) **245**, 37 (1996)
31. E.T. Jaynes: Phys. Rev. **108**, 171 (1957); *ibid.* **108**, 620 (1957) 620; Am. J. Phys. **31**, 66 (1963)
32. J.N.Kapur and H.K.Kesavan: *Entropic Optimization Principles with Applications* (Academic Press, New York, 1992)
33. A. Katz: *Principles of Statistical Mechanics* (W.H. Freeman and Company, San Francisco, 1967)
34. A. Hobson: *Concepts in Statistical Mechanics* (Gordon Breach Science Publishers, New York, 1971)
35. H. Jeffreys: *Theory of Probability*, 3rd ed (Oxford Univ. Press, Oxford, 1960); R. von Mises: *Mathematical Theory of Probability and Statistics* (Academy Press, New York, 1964)
36. U. Leonhardt and M. Munroe, Phys. Rev. A **54**, 3682 (1996)
37. I. Bouchoule, H. Perrin, A. Kuhn, M. Morinaga, and C. Salomon: Phys. Rev. A **59**, R8 (1999)
38. M. Morinaga, I. Bouchoule, J.-C. Karam, and C. Salomon: Phys. Rev. Lett. **83**, 4037 (1999)
39. We should stress that due to random fluctuations of "observed" mean values (6.73) physically incompatible data might be obtained. It means that there does not exist a physical density operator which could fit perfectly the results of the noisy measurement (i.e. leading to $\Delta F \to 0$). Obviously increasing the relative error of the measurement we increase also a number of incompatible results and the reconstruction becomes meaningless.
40. C. Salomon and I. Bouchoule: private communication
41. B.-G. Englert, N. Sterpi, and H. Walther: Opt. Commun. **100**, 526 (1993)
42. L.G. Lutterbach and L. Davidovich: Phys. Rev. Lett. **78**, 2547 (1997)
43. C. Cohen-Tannoudji, J. Dupont-Roc, and G. Grynberg: *Atom-Photon Interactions* (John Wiley & Sons, New York, 1992)
44. N.F. Ramsey: *Molecular Beams* (Oxford University Press, New York, 1985)
45. P. Bertet, A. Auffeves, P. Maioli, S. Osnaghi, T. Meunier, M. Brune, J.M. Raimond, and S. Haroche: Phys. Rev. Lett. **89**, 200402 (2002)
46. J.M. Raimond, M. Brune, and S. Haroche: Rev. Mod. Phys. **73**, 565 (2001)
47. E. Skovsen, H. Stapelfeldt, S. Juhl, and K. Molmer: Phys. Rev. Lett. **91**, 090406 (2003)